PNL-7345
UC-313

18J

Inert Electrode Program

Results from Electrolysis Test of a Prototype Inert Anode

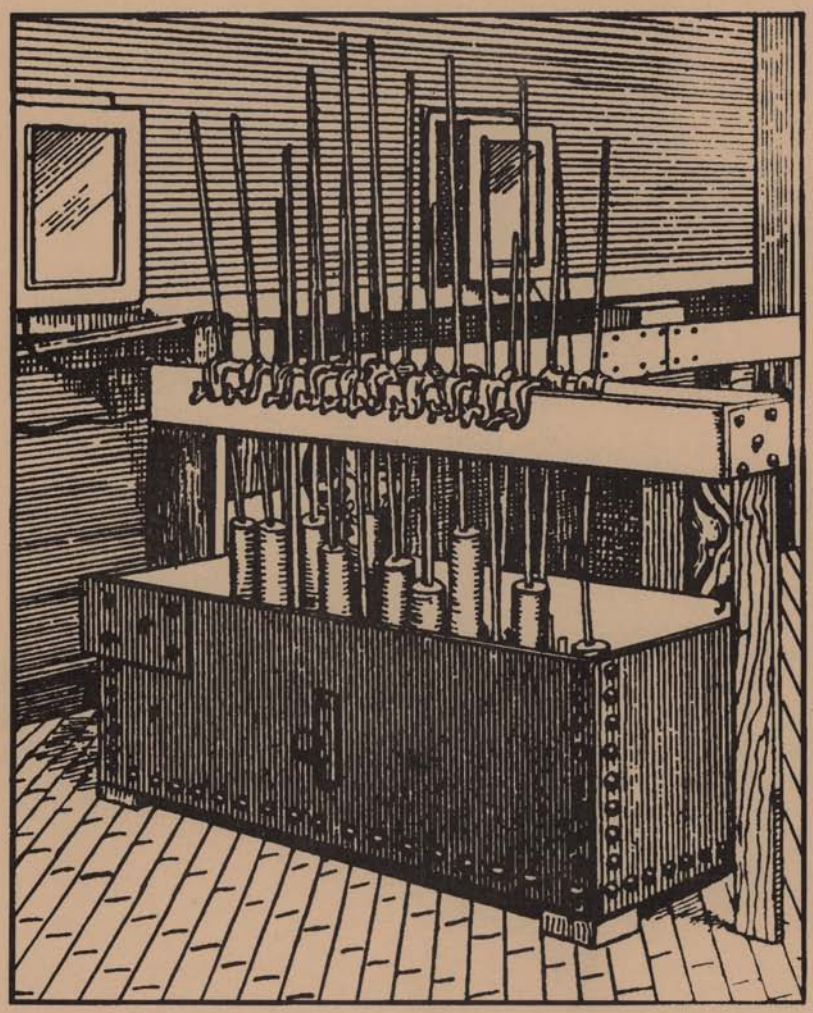

May 1990

Work Supported by the U.S. Department of Energy
under Contract DE-AC06-76RLO 1830

Pacific Northwest Laboratory
Operated for the U.S. Department of Energy
by Battelle Memorial Institute

Battelle

PNL-7345

On the cover:

Aluminum reduction pots at the Pittsburgh Reduction Company's (Alcoa's) plant in 1889. Adapted from a photograph, courtesy of Alcoa.

DISCLAIMER

This report was prepared as an account of work sponsored by an agency of the United States Government. Neither the United States Government nor any agency thereof, nor Battelle Memorial Institute, nor any of their employees, makes any warranty, expressed or implied, or assumes any legal liability or responsibility for the accuracy, completeness, or usefulness of any information, apparatus, product, or process disclosed, or represents that its use would not infringe privately owned rights. Reference herein to any specific commercial product, process, or service by trade name, trademark, manufacturer, or otherwise, does not necessarily constitute or imply its endorsement, recommendation, or favoring by the United States Government of any agency thereof, or Battelle Memorial Institute. The views and opinions of authors expressed herein do not necessarily state or reflect those of the United States Government or any agency thereof.

PACIFIC NORTHWEST LABORATORY
operated by
BATTELLE MEMORIAL INSTITUTE
for the
UNITED STATES DEPARTMENT OF ENERGY
under Contract DE-AC06-76RLO 1830

Printed in the United States of America

Available to DOE and DOE contractors from the
Office of Scientific and Technical Information, P.O. Box 62, Oak Riie, TN 37831;
prices available from (615) 576-8401. FTS 626-8401.

Available to the public from the National Technical Information Service,
U.S. Department of Commerce, 5285 Port Royal Rd., Springfield, VA 22161.

NTIS Price Codes, Microfiche A01

Printed Copy

Price Code	Page Range
A02	1- 10
A03	11- 50
A04	51- 75
A05	76-100
A06	101-125
A07	126-150
A08	151-175
A09	176-200
A10	201-225
A11	226-250
A12	251-275
A13	276-300
A14	301-325

Price Code	Page Range
A15	326-350
A16	351-375
A17	376-400
A18	401-425
A19	426-450
A20	451-475
A21	476-500
A22	501-525
A23	526-550
A24	551-575
A25	576-600
A99	601-Up

3 3679 00056 9642

PNL-7345
UC-313

RESULTS FROM ELECTROLYSIS TEST OF A PROTOTYPE INERT ANODE

D. M. Strachan
C. F. Windisch, Jr.
O. H. Koski
L. G. Morgan
R. D. Peterson[a]
N. E. Richards[a]
A. T. Tabereaux[a]

May 1990

Prepared for
the U.S. Department of Energy
under Contract DE-AC06-76RLO 1830

Pacific Northwest Laboratory
Richland, Washington 99352

(a) Reynolds Metals Company Manufacturing Technology Laboratory, Sheffield, Alabama

SUMMARY

Reynolds Metals Co. Manufacturing Technology Laboratory and the Pacific Northwest Laboratory (PNL) conducted the first in a series of electrolysis tests with a prototype-scale cermet anode for the production of aluminum. The objective was to determine if an anode produced by a commercial vendor from components provided by PNL could survive in a test under conditions approximating those found in a commercial electrolysis cell.

The 15-cm-diameter by 20-cm-high anode was instrumented to collect volt/amp signatures for calculations that would provide information on simplified anode control strategy. The anode was tested for 113.5 hours in alumina-saturated electrolyte with no major operational difficulties.

Although an oxygen-evolving electrode should have a higher decomposition voltage than a graphite anode, it appears that the cermet anode voltage drop and overpotential are considerably lower than anticipated. High levels of impurities (~8% near the end of the test) were picked up by the molten Al in the cell. The cermet anode suffered corrosion, which resulted in a decrease of approximately 6 mm in the diameter of the anode. Frozen electrolyte and accumulated Al_2O_3 appear to have protected the anode in the region of the anode-air-electrolyte interface.

The test was conducted with several differences from the 20-h laboratory-scale tests performed earlier at PNL. Further testing is currently under way at PNL in an attempt to determine which, if any, of these differences may have contributed to the more extensive corrosion of the anode in the prototype-scale test.

CONTENTS

1.0 INTRODUCTION 1.1

2.0 CONCLUSIONS 2.1

3.0 EXPERIMENTAL METHODS AND EQUIPMENT 3.1

3.1 ANODE 3.1

3.1.1 Anode Construction 3.1

3.1.2 Pre-Test Characterization 3.2

3.2 ELECTROLYSIS CELL 3.3

3.2.1 Cell Construction 3.3

3.2.2 Monitoring Equipment 3.6

3.2.3 Cell Operation 3.6

3.2.4 Inert Anode Preheat and Transfer 3.11

3.2.5 Signal Monitoring 3.12

3.3 CHEMICAL ANALYSES 3.15

3.3.1 Bath Ratio 3.15

3.3.2 Alumina Analyses 3.17

3.3.3 Trace Element Analyses 3.17

3.3.4 Calcium Content of the Electrolyte 3.18

3.3.5 Impurity Resulting from Dissolution of Reference Electrodes 3.18

3.3.6 Chemical Composition of the Anode 3.18

3.4 SOLID-STATE ANALYSES 3.19

3.4.1 Scanning Electron Microscopic Analyses 3.19

3.4.2 X-Ray Diffraction Analyses 3.19

4.0 RESULTS AND DISCUSSION 4.1

4.1 CELL OPERATION 4.1

4.1.1 Electrical Results 4.1

4.1.2 Electrolyte Chemistry and Temperature 4.6

4.1.3 Metal Purity 4.11

4.1.4 Cell Mass Balance 4.13

4.2 ANODE CHARACTERIZATION 4.14

4.2.1 Anode Rim 4.16

4.2.2 Melt Line 4.21

4.2.3 Electrolysis Surfaces 4.22

4.2.4 Electrical Connection 4.23

4.3 SIGNAL MONITORING 4.25

4.3.1 Digital Signal Analysis 4.25

4.3.2 Analog Data Analysis 4.33

4.3.3 Reference Anode 4.33

5.0 REFERENCES 5.1

APPENDIX _ MASS BALANCE FOR THE CELL A.1

FIGURES

1.1 Prototype Anode Prior to Testing and After Machining 1.2

3.1 Top Rim of Anode 3.3

3.2 Inert Anode Test Cell 3.4

3.3 Wiring Diagram 3.7

3.4 Furnace Preheat Cycle 3.11

3.5 Sensor and Instrument Assembly for Digital Signal Measurement 3.13

3.6 Strip Chart Recorder Arrangement 3.16

3.7 Composition of Cu/Ni Alloy by XRD Line Position 3.20

4.1 Cell Current and Voltage During Graphite Anode Run 4.2

4.2 Current Scan of Graphite Anode Electrolysis 4.2

4.3 Current and Voltage During Inert Electrode Run 4.3

4.4 Current Scan at 4.4 h of Inert Anode Electrolysis 4.3

4.5 Cell Voltage Due to Bubble Effect 4.5

4.6 Temperature History for the Prototype Anode Test Cell 4.7

4.7 Summary of the Bath Ratios for the Electrolyte in the Prototype Anode Test 4.7

4.8 Results from Analyses of the Dissolved Al_2O_3 in the Electrolyte Used in the Prototype Anode Test 4.8

4.9 Results from the Analyses of Cu, Fe, and Ni in the Electrolyte Used in the Prototype Anode Test 4.8

4.10 Copper. Iron. and Nickel Concentrations in the Metal During the Prototype Anode Test 4.12

4.11 Comparison of Observed Impurity Ratio in Al Metal with Impurity Ratio in Cermet 4.13

4.12a Prototype Anode After Testing 4.15

4.12b Bottom Face of the Prototype Anode Showing the Cracks That Developed During the Test 4.15

4.13 Photograph Showing the Used Prototype Anode in Cross Section and the Places at Which Samples Were Taken for Solid-State Analyses 4.16

4.14 Upper Portion of the Prototype Anode Rim Showing the Degree of Oxidation 4.17

4.15 Results from the XRD Analysis of the Oxidized Rim Material from the Prototype Anode After Testing 4.18

4.16 SEM Photomicrograph of the Cermet Portion of the Oxidized Rim of the Prototype Anode 4.19

4.17 Photomicrograph at Larger Magnification of a Grain Shown in Figure 4.16 . . . . . 4.20

4.18 SEM Photomicrograph of the Immediate Surface of the Oxidized Rim Material on the Prototype Anode 4.21

4.19 Results from the XRD Analysis of the Immediate Surface of the Oxidized Layer of the Prototype Anode Rim 4.22

4.20 Photomicrograph of the Prototype Anode at the Melt Line. 4.23

4.21 Photomicrograph of the Prototype Anode Electrolysis Surface. . . 4.24

4.22 Results from the XRD Analysis of the Oxidized Material on the Electrolysis Surface of the Prototype Anode 4.25

4.23 Results from Energy Dispersive X-Ray Analyses in the SEM of the Metallic Phase near the Electrolysis Surface. 4.26

4.24 Photomicrograph of the Electrical Connection Area of the Prototype Anode 4.27

4.25 SEM Photomicrograph at Higher Magnification of the Electrical Connection Shown in Figure 4.24 . . . . . 4.28

4.26 SEM Photomicrograph at Higher Magnification of the Area Shown in Figure 4.25. . . . . 4.28

4.27 Parameter P(l)/R(o): Comparison for Prototype Anode Data B Low-Passed Voltage Signals. 4.30

4.28 Parameter P(l)/R(o): Comparison for Prototype Anode Data C Low-Passed Voltage Signals. 4.30

4.29 Parameter R(o): Comparison for Prototype Anode Data B Low-Passed Voltage Signals. 4.31

4.30 Parameter R(o): Comparison for Prototype Anode Data C Low-Passed Voltage Signals 4.31

4.31 Corrosion of Reference Anode 4.34

TABLES

3.1 Shift Tasks 3.8

3.2 Target Operating Conditions 3.9

3.3 Impurities of Test Constituents 3.10

3.4 Descriptions of Conditions at Data Collection Times 3.14

4.1 Cell Voltage Breakdown for Graphite Anode 4.6

4.2 Cell Voltage Breakdown for Ferrite Anode. 4.6

A.1.1 Mass Balance Sheet and Results from Analyses of Electrolyte Samples A.1

A.1.2 Results from Duplicate Analyses of Selected Electrolyte Samples A.5

A.2 Results from Analyses of Al Metal Samples A.6

1.0 INTRODUCTION

Nonconsumable or inert anodes are being developed at the Pacific Northwest Laboratory (PNL) [a] for use in the electrolytic production of aluminum. A series of laboratory tests on the laboratory scale (Hart et al. 1987; Strachan et al. 1989; Marschman 1989) has shown the technology to be potentially feasible. A series of larger-scale experiments are now being run to determine the viability of the technology on a commercial scale.

The results reported here are from a test performed at the Reynolds Metals Company, Manufacturing Technology Laboratory, Sheffield, Alabama, using a prototype anode. The prototype anode was approximately 15 cm in diameter and 20 cm high (Figure 1.1). The objectives of the test were to determine if an anode, produced by a commercial vendor, could survive in a test under conditions approximating those found in a commercial electrolysis cell; to familiarize the Reynolds staff with the operation of such an anode in a subsequent pilot cell test of the inert anode technology; and to familiarize the PNL staff with the operations at the Reynolds Metals Company facility.

The anode test was highly instrumented, more instrumented than an anode under projected normal use, to provide a means for gathering information beyond that collected using a laboratory electrolysis cell. Information was collected on the macroscopic and microscopic properties of the anode before and after the test. Also, during the test, volt/amp signatures were collected to perform calculations that would provide information, normally hidden, on the behavior of the anode in the cell. Such information could lead to improved and/or simplified control strategies for industrial electrolysis cells.

While this instrumented anode was approximately a factor of 40 more massive and had a factor of 10 larger surface area than the anodes studied earlier at PNL, several constraints were placed on the interpretation of the

---

(a) Operated for the U.S. Department of Energy by Battelle Memorial Institute under Contract DE-AC06-76RLO 1830.

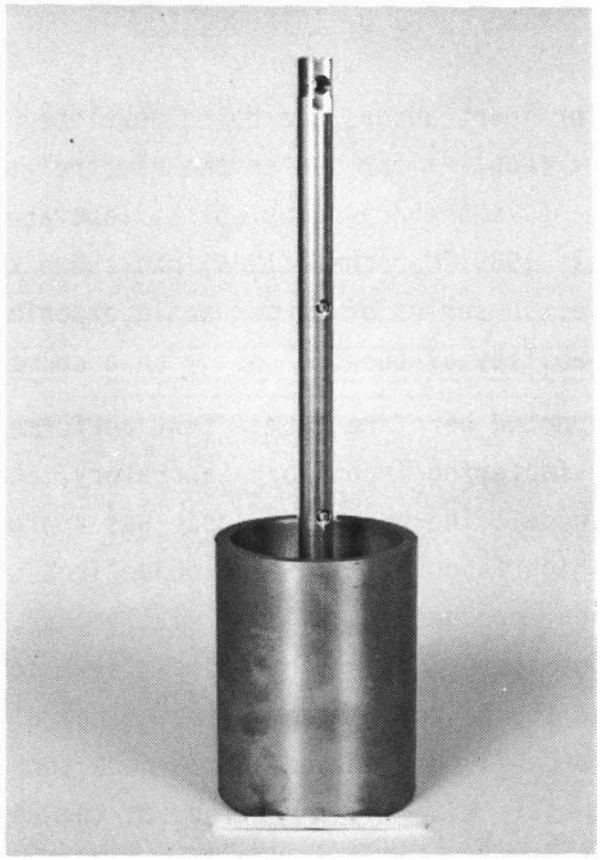

FIGURE 1.1. Prototype Anode Prior to Testing and After Machining

data from this cell because of the small size relative to a pilot cell. Some of these limitations included the interpretation of the metal purities, anode corrosion, and cell control. The metal purities that will be discussed later are not believed to be representative of the purities that may result in a much larger cell because of the high anode surface area-to-molten aluminum surface area. Anode corrosion may not be fully understood because the cell construction may have contributed to the observed corrosion. In a pilot cell facility, such interactions may not be present and may be more representative of an actual industrial cell.

The test reported here is the result of a cooperative effort between Reynolds Metals Company and PNL. The test was begun at the Manufacturing Technology Laboratory on March 19, 1989, and ended on March 25, 1989. Several of the chemical analyses were performed at the Reynolds facility and

some were performed at PNL. Some of the analyses performed at Reynolds were duplicated at PNL. Principally, the post-test efforts at PNL centered on obtaining a full understanding of the anode performance through solid-state analyses.

Current and voltage data were also collected during the test. Analog current and voltage signals were used to evaluate the stability of the operation of the prototype anode while the test was being performed. Digital current and voltage signals were analyzed at a later date to determine whether digital signal analysis (DSA) methodology could be used to monitor and control aluminum smelting operations involving inert anodes. The digital signal data were analyzed by Dr. Chrysostomos L. Nikias, Northeastern University, Boston, Massachusetts, under a subcontract with PNL.

2.0 CONCLUSIONS

The common goal shared by both the industrial participants in the prototype anode test and the research and development scientists is to implement inert anode techno1ogy and revitalize the aluminum smelting business. In pursuit of this common goal, however, the two groups have separate sets of interests. Therefore, the two different perspectives on the outcome of the test are discussed separately.

INDUSTRIAL PERSPECTIVE

From the standpoint of an aluminum producer such as Reynolds, the test was found to be a qualified success. The inert anode met the 100-h test criterion despite serious material problems, but the anode is not yet ready for an industrial application. Further testing is required to more accurately determine the long-term performance of the inert anode in commercial cells. The industrial interests and conclusions are as follows.

Transfer of the Anode from a Preheating Furnace to the Cell

The prototype anode was successfully transferred while hot from a preheating furnace to a hot electrolytic cell. This was accomplished under the controlled conditions of the laboratory. Changing anodes in a pilot cell will be more difficult and require more detailed planning.

Durability of the Prototype Anode

The prototype anode material showed signs of attack, but it lasted well over the 100-h target time for use in the electrolytic cell. A major area of concern is the spalling of the upper anode surfaces. This may not occur in the pilot cell where the upper portions of the anode are predicted to be within the cold cap overlying the pilot cell electrolyte. Other areas of concern are the apparent mismatch in the coefficients of thermal expansion, which is thought to have caused the cracks in the anode, and the apparent severe corrosion of the anode material.

Cell Voltages with an Inert, Oxygen-Evolving Anode

The major difference between the graphite and ferrite-based anode systems lies in the anode surface reaction, which is manifested in two ways: overvoltage and decomposition voltage. The overvoltage associated with the ferrite-based anode is considered to be minimal (<0.1 V versus an estimated 0.46 V for the graphite anode at 120 amps), but the decomposition voltage is higher (2.22 V versus 1.19 V) for the oxygen-evolving inert anode. The voltage drop associated with anode resistance is also smaller with the ferrite-based anode since it is a better electrical conductor than the graphite. Based on cell current scan measurements under similar conditions, the graphite anode had a cell voltage of 3.781 V at 120 amps compared with 3.603 V for the ferrite anode. It should be noted that the inert anode may have been conducting current through a different path during its use and this may have affected the current scan data. Results indicate that the conduction path may have been shorter during the prototype anode portion of the test when the electrolyte voltage was measured, since the alumina liner appeared to have dissolved, thereby exposing the cathode side walls and yielding a slightly lower value for the cell voltage. Overall, the voltage associated with the inert anode seems to be very close to that currently associated with carbon electrodes.

Contamination of the Al Metal

In this test, high levels of Cu, Fe, and Ni were picked up by the molten Al in the cell. A total impurity level of ~8% was found near the end of the test. This value may not be characteristic of operation in a normal commercial cell. Some of the impurities came from ferrite reference electrodes that fell into the metal pool. Additionally, the ratio of the mass of the anode to the mass of metal pool is not the same in the test cell as it would be in a commercial cell. The high ratio intensifies the tendency of the metal pool to pick up impurities. Although anode material was definitely lost to the system, the total contamination concentration observed is higher than would be expected in a commercial cell.

Effect of Evolving Oxygen on Cell Components

As long as the electrolyte covered the graphite, there were no problems of attack on cell components. A test with a graphite rod showed that oxygen was not "carried" under the electrolyte surface. In a commercial cell, provisions may have to be made for the protection of the upper carbon side wall either by changing materials of construction, by maintaining a frozen crust of electrolyte as a protective cover, or by some other strategy.

Contribution of the Anode Side Wall to the Overall Anode Current Density

Examination of the voltage components before and after anode movements indicated that the submerged anode side walls were carrying a significant portion of the current. Post-test examination of the prototype anode also indicated that the side wall was carrying a significant portion of the current. At this point, the exact amount of current and the relationship between the side wall contribution and the bottom face contribution are not clearly known. Further work is needed in this area.

MATERIALS RESEARCH PERSPECTIVE

Complete microstructural and chemical analyses were completed on the cermet prototype anode that was used in the electrolysis test for 113 h. Interests and conclusions from a materials research perspective are as follows.

Amount of Corrosion

The anode suffered corrosion, which resulted in a decrease of approximately 6 mm in the diameter of the anode. A rind of oxidized cermet material was formed on the surface of the anode at various thicknesses.

Analyses of the metallic phase as a function of depth to the interior of the anode from the oxidized rind suggested the types of changes the anode material underwent during polarization. To the interior of the anode from the surface rind was a zone of copper-colored material. Using x-ray diffraction (XRD) and chemical analyses, it was concluded that the copper color resulted from selective oxidation of the Ni from the metallic phase in the cermet. Although it is not known at what percentage Cu a Cu/Ni alloy becomes

copper-colored, Cu/Ni alloys below 70 mass% Cu are, like the starting alloy in the cermet, silver-colored. From the XRD analyses, it was determined that the composition of the metallic phase approached pure Cu in the regions where the Cu color existed. It is not known if the selective oxidation of the Ni from the Cu/Ni metal phase in the cermet has any beneficial effect on overall performance of the anode or if a pure Cu metal phase would enhance performance.

Oxidation on the Surface of the Anode

Oxidation of the cermet surface above the electrolyte was extensive and probably resulted in some spalling of material during the test. The oxidation rind was thickest in this region. Results from XRD show that the Cu was oxidized to CuO. Copper and Ni appeared to be selectively volatilized, leaving behind a more Fe-rich material. Iron also was undoubtedly lost from this region.

Below the electrolyte, the oxidation rind on the surface of the anode was approximately 3 mm thick. Results from XRD show that the Cu was oxidized to Cu_2O in this region.

In the region of the anode-air-electrolyte interface, the rind of oxidized cermet and the copper-colored zone were thinnest. Frozen electrolyte and accumulated Al_2O_3 appear to have protected the anode, acting as a barrier to the migrating oxidant, at least in the region of the anode-air-electrolyte interface.

Possible Explanations for Increased Amount of Corrosion

In many of the 20-h tests performed at PNL the anodes have suffered little or no corrosion (Hart et al. 1987; Strachan et al. 1988, 1989). What caused the dramatically increased corrosion in this test is, at present, uncertain. However, there were several differences between the test as performed at the Reynolds Metals Company and the PNL tests.

One of the primary differences was the preheating of the anode before testing. In the laboratory tests at PNL, the anodes were preheated along with the electrolysis cell. At Reynolds, the anode was preheated in a box

furnace separate from the electrolysis cell. This approach was taken because a graphite anode was to be used before using the cermet anode.

Another difference was the presence of SiO_2 in the electrolyte. At PNL the top of the electrolysis cells are loosely covered with boron nitride plates or other insulating board. During the test at Reynolds, a ceramic fiber-based material was used to insulate the top of the furnace. When the cell lid was opened to remove samples from the cell or to inspect the anode and environment, invariably some of this insulation fell into the cell. Earlier work (Weyand et al. 1986) suggested that the presence of dissolved SiO_2 in the electrolyte was deleterious to anode performance. Although Si was found in the electrolyte samples taken during the test, it is uncertain if sufficient SiO_2 was present in the electrolyte to enhance anode corrosion.

Surface treatment was also suggested as a possible cause of corrosion. When the anode was manufactured, insufficient O_2 was present during the sintering process. This produced a thin rind of material on the surface of the anode which was removed using a diamond grinding wheel. During the laboratory testing of cermet anodes, several anodes were reshaped after sintering (Marschman 1989). These anodes exhibited little or no corrosion in 20-h tests and yielded metal of excellent quality. Therefore, it seems unlikely that the process of surface treatment i.e., grinding, contributed to the enhanced corrosion observed in this test. Results from the XRD and chemical analyses indicate that the material was essentially the same as that used in the laboratory tests. However, the electrical conductivity of the anode tested was slightly different, suggesting some differences may have existed.

Further testing is currently under way at PNL in an attempt to determine which of the above factors affect anode corrosion. These tests will be completed before a pilot-scale test of the cermet anodes is performed so that changes in the test procedures can be made and/or materials problems identified and solved.

3.0 EXPERIMENTAL METHODS AND EQUIPMENT

This section describes the anode and electrolysis cell, along with the chemical and solid-state analyses conducted during and after the experiments, and the signal monitoring methods.

3.1 ANODE

The anode used in this test was produced at Cercom, Inc., Vista, California, according to a recipe used at PNL and modified to take into account the large size of this anode relative to the size of the laboratory-scale anodes. The powders for this anode were supplied by PNL and were the same powders used in making the laboratory-scale anodes. After the anode was produced, it was sent to PNL for nondestructive testing and then sent to the Reynolds facility in Sheffield where it was assembled and tested.

3.1.1 Anode Construction

Powders consisting of a spray-dried ferrite powder (designated 5324 and produced for PNL at Stackpole Carbon, Pittsburgh, Pennsylvania) and separate fine Cu powder (Cerac Inc., Milwaukee, Wisconsin) were sent to Cercom to be blended and sintered into anodes. The 5324 powder had a nominal composition of 51.7 mass% NiO and 48.3 mass% Fe_2O_3. The 5324 powder was then blended with very fine Cu powder, 83 mass% 5324 and 17 mass% Cu. This powder blend was then loaded into an isostatic press mold and pressed at 170 MPa (25000 psi). The green anode was sintered in an internally heated, SiC heating element furnace. The oxygen level was controlled at the entrance and monitored at the entrance and the exit to the furnace to obtain the correct sintering atmosphere.

Several runs were conducted, including one in which a full-sized anode was made, before the prototype anode was actually produced. Small samples were included in the early sintering'runs, which were sectioned and examined to determine if the sintering conditions were yielding a good product. A portion of the rim of the final anode was removed for later examination. In all cases, including the final sintering run, the oxygen content in the furnace was too low during all or part of the sintering cycle. The low

oxygen content yielded an area at the surface of the final anode that needed to be removed by machining with a diamond-impregnated wheel. Anodes had been machined before use during the laboratory testing, and enhanced corrosion was not a problem (Marschman 1989). The appearance of the anode once the surface had been ground can be seen in Figure 1.1.

3.1.2 Pre-Test Characterization

The anode as received from Cercom was examined nondestructively using x-ray radiography. The detection limit using this technique are flaws (cracks, voids, etc) about 1 mm in size. Reproductions of the radiographs are not shown here because of the poor photographic quality.

When the anode arrived at PNL, the hole for the electrical connection in the bottom-center of the anode was not straight, which would have caused the nickel rod used for the connection to the electrical bus to be at an angle relative to the anode support and to the working face of the anode. To correct the angle of the connecting nickel rod the hole was drilled larger, tapped, and a nickel bushing inserted to center and straighten the nickel rod.

Potentially, the large anode could have been different from those produced in the laboratory because the atmosphere could not be controlled in the large furnace at Cercom as it could be in the laboratory furnace. It was observed that to obtain approximately 200 ppm 0, in the Ar gas at the outlet of the large furnace, more than 5500 ppm 0, was needed at the inlet. High O_2 losses in the furnace were noted even without any anode material present. It was uncertain what effect this had on the overall properties of the large anode, but the piece cut from the top rim of the anode clearly indicated the presence of a metal-rich rind (Figure 3.1). This rind was removed during the surface grinding mentioned above. The final dimensions for the anode were 14.9 cm in diameter and 20 cm high. The anode had a mass of 11.959 kg.

Examination of the sample taken from the rim of the anode indicated that NiO had been reduced to Ni. Under examination in the scanning electron microscope (SEM), the amount of NiO present in the affected area of the cermet was less than that found in the cermet immediately adjacent to the rind. There was also evidence that the Ni content of the ferrite phase

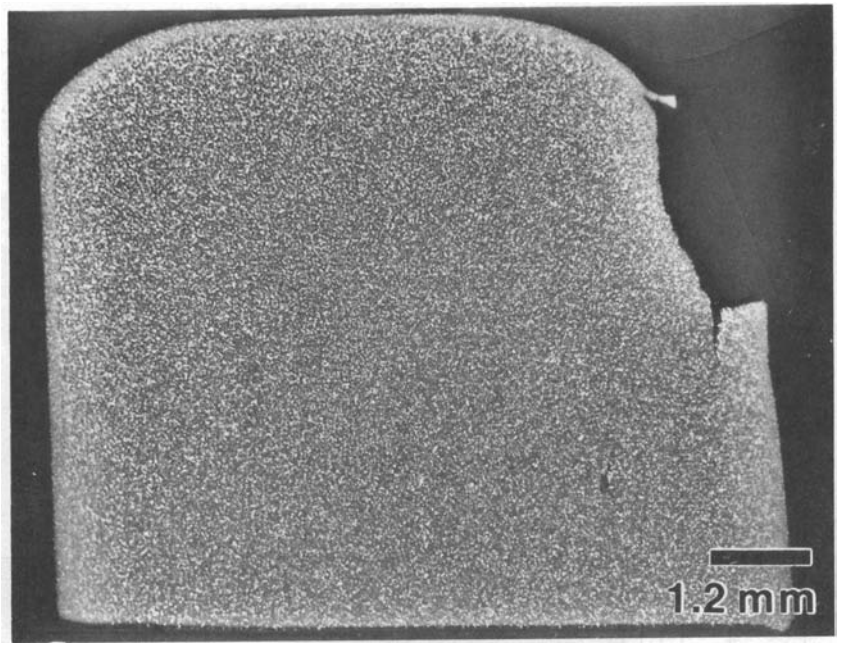

FIGURE 3.1. Top Rim of Anode

($NiFe_2O_4$) was greater in the rind than interior to the anode. This phase is known to have a variable stoichiometry and can accommodate more Ni. The chemical formula for this phase should more properly be written as $Ni_xFe_{3-x}O_4$. These phases all have the spinel structure. However, in this report the ideal stoichiometry ($NiFe_2O_4$) is used. An increase in porosity was also noted in the rind (Figure 3.1).

3.2 ELECTROLYSIS CELL

3.2.1 Cell Construction

Under the operating conditions of the laboratory test, the cell would not be thermally self-sustaining. Therefore, the test was conducted in an electrically heated furnace. The largest suitable furnace at the Reynolds facility had a minimum cross-sectional dimension of 48 cm. This constraint and the diameter of the anode defined the size of the containing crucible and most of the other test components.

A schematic of the test cell is shown in Figure 3.2. The graphite crucible had an outside diameter of 38 cm and an inside diameter of 24.8 cm.

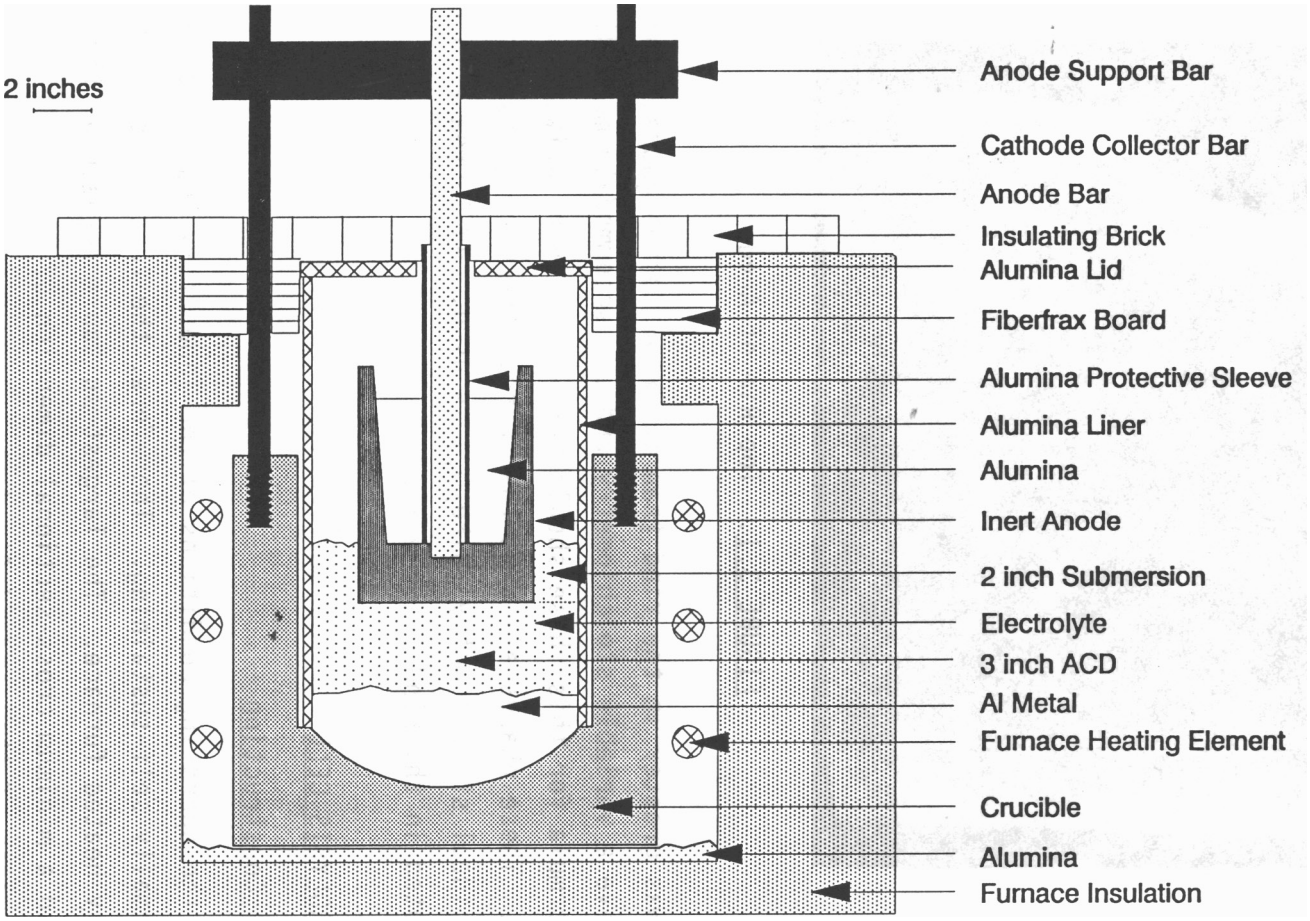

FIGURE 3.2 Inert Anode Test Cell

The bottom of the graphite crucible had a ledge upon which the alumina liner rested and had a spherical shape to minimize thermally induced stresses during heat-up. The spherical shape also served as a location to which cell muck could settle during the test.

The alumina liner had a nominal internal diameter of 23 cm and a nominal wall thickness of 6 mm. The liner was 25 cm in height. The upper portion of the liner prevented the oxygen that was generated at the anode from coming into contact with the graphite crucible or the furnace interior. An alumina plate with various access holes was placed on top of the alumina liner to reduce thermal and vapor losses during cell operation.

Two 316 stainless steel collector rods, 2.5 cm in diameter, were used for electrical connection to the cathode crucible. These rods were threaded into the upper surface of the crucible opposite each other. The upper ends of the rods were connected by an anode hanger constructed from a 5 cm by 12 mm steel bar. In addition to supporting the anode assembly, this bar was used to raise and lower the entire crucible assembly into the furnace. Electrical connections were made to both cathode rods to ensure good current distribution to the cell. The cathode was also drilled for a thermocouple so that the temperature could be monitored continuously.

The cell assembly was placed in a SiC heating element furnace. The volume above the upper edge of the crucible and extending to the furnace wall was filled with fibrous aluminosilicate wool boards (Figure 3.2). These boards acted as thermal insulators as well as barriers to minimize infiltration of atmospheric oxygen. Additionally, the lower furnace cavity was purged with industrial-grade argon at a rate of 510 to 1020 standard m^3/s (5 to 10 SCFH) to retard the oxidation of the Inconel* outer crucible. A separate argon purge line provided argon to the anode area of the cell to reduce the oxygen partial pressure. The crucible was coated with a boron nitride paint to further retard surface reactions. The upper surface of the furnace was covered with lightweight, high insulating fire brick as a final

---

* Inconel is a registered trademark of Huntington Alloys (INCO Alloys International), Huntington, West Virginia.

insulating barrier. These bricks could be removed from the area over the crucible interior so that measurements and samples could be taken.

A 3.2 cm ID alumina tube was slipped over the Ni rod attached to the cermet anode to minimize corrosion of the Ni rod. The thermocouple, anode tap, and connector tap wires were also threaded through the alumina sleeve. This protective sleeve protruded above the top of the furnace. The nickel rod was insulated from the anode hanger bar and the cathode connections by a boron nitride insulating ring.

The wiring diagram for the power supply to the cell is shown in Figure 3.3. A 200 A, 20 V power supply was used (Model 6453A, Hewlett-Packard, Huntsville, Alabama). The system voltage was measured at the power supply backplane. The bus cable was bolted to the cell leads and was made of heavy gauge copper welding cables with crimped ring connections. A shunt was used to measure cell current; the signal output was 100 mV for 200 A.

3.2.2 Monitoring Equipment

A Doric data logging system (Model Digitrend 235, Doric Corp., San Diego, CA) was used to record the cell voltage; cell current; and cathode, anode, cell, and anode connector temperatures. These data were then downloaded to a computer (Compaq Portable 386, Compaq Computer Corp, Houston, Texas) once every minute where the data were stored on a floppy disk for later retrieval. All data acquisition equipment was calibrated to Reynolds Metals Company Quality Assurance standards.

3.2.3 Cell Operation

The cell was first operated with a graphite anode so that personnel could become familiar with the operation of this cell, work out any operational idiosyncrasies, and have a basis for comparison of the two anodes. During this time, the electrolyte composition was adjusted, and sampling procedures and schedules were defined. During each shift, the personnel had to collect data not gathered by the data logging system or had to maintain the cell in a stable operating mode. These tasks and the frequency at which they were performed are outlined in Table 3.1. All probing of the cell was

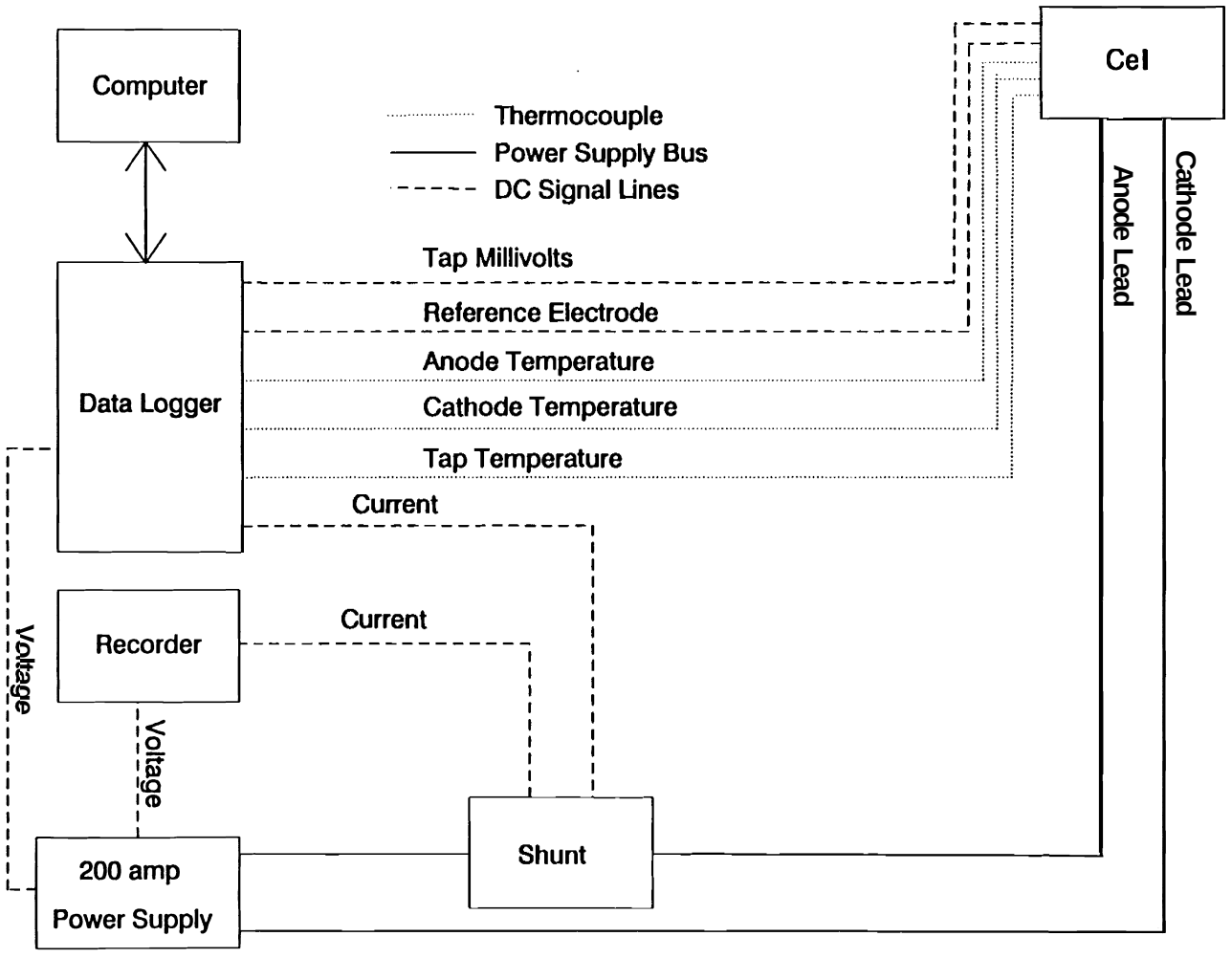

FIGURE 3.3 Wiring Diagram

TABLE 3.1. Shift Tasks

Intervals	Tasks
Hourly	Log cell voltage, cell current, cell temperatures total amp-hours. Check cell for muck and add appropriate amount of alumina. Check argon cylinders.
Every 4 Hours	Measure anode immersion depth. Measure anode-to-cathode distance. Make additions to electrolyte if necessary. Measure electrolyte temperature. Collect metal and electrolyte samples.
Every 8 Hours	Measure bath ratio by pyro titration. Conduct amp-voltage scan. Measure individual cell voltage components.

conducted with molybdenum, tungsten, or graphite tools to minimize contamination of the electrolyte and metal with impurities common to the anode. Target conditions (Table 3.2) were set for the operation of both the carbon and inert anodes and, generally, these conditions were the same.

The major difference in operational procedure between the two anodes was in the cell current. The inert anode was to be operated at a current density no higher than 0.5 A/cm^2 for stability reasons. A graphite anode can be operated at very high current densities with little problem. Current density was used to calculate the total cell current. A difficulty arose when the calculation of the total current was attempted because a current flux must be ascribed to the side walls of the anode. Depending on how much of the current flows through the side walls (long path to the cathode) and the bottom (short path to the cathode) of the anode, the target current density could be exceeded. Two extreme cases for current distribution were considered: the side walls carried no current, or the side walls carried the same current as the bottom face. Obviously, the real current distribution was between these two extremes. For the conditions of operation present in this cell, the area of the side walls was 33% larger than the area of the bottom face. Consequently, the contribution of the side walls to the total current made a large difference in the calculation of total cell current.

TABLE 3.2. Target Operating Conditions

Parameter	Graphite Anode	Ferrite Anode
Bath Ratio	1.35	1.35
%CaF_2	5.0	5.0
Al_2O_3	To anode effect, then saturated	Saturated
Current	172.5	As specified by PNL
ACD	>7.5 cm	>7.5 cm
Immersion Depth	5 cm	5 cm

One way to calculate the current distribution is by modeling the cell geometry and electrolyte conductivity. This type of calculation was carried out by Dr. Uziel Landau, Case Western Reserve University, Cleveland, Ohio. His calculations showed that, compared with the flatter sections of the anode, sharp corners will exhibit a significantly larger current density while rounder corners will not. Also, compared with the flat-bottomed surface, the electrode side walls will carry very little current. While the first conclusion was supported by patterns of anode corrosion observed in laboratory tests, the second was at variance with some of the PNL laboratory tests, which have shown a dependence of current density on the depth of anode immersion and hence on the side-wall surface area. For this reason, another approach was taken to determine the side-wall contribution to the total current.

In the PNL approach, the two surface types on the cylindrical anode, the flat-bottomed surface and the side walls, were associated with their own independent portions of the cell current. The portions were modeled by two resistors in parallel. This approach, while approximate, yielded calculated current density values that were more consistent with observed anode behavior.

After the crucible was positioned in the furnace and sealed in place with refractory board, a total of 4.700 kg of Al metal were added to make the

metal cathode pool. The Al was spherical shot with an overall purity of 99.75%. The trace impurities in the Al are shown in Table 3.3. The addition of 4.700 kg of metal created a pool that filled the curved portion of the crucible and the bottom 3.2 cm of the alumina liner.

A cryolite-based electrolyte was made to have a bath ratio of 1.35, 5% CaF_2, and 8% Al_2O_3. An industrial electrolyte was used as the base material to which additional CaF_2 and NaF were added to adjust the chemistry. The actual concentration of alumina in the electrolyte was higher than the target of 8% because of abnormally high amounts of Al_2O_3 in the industrial electrolyte. The trace impurities in the electrolyte are also shown in Table 3.3. A total of 11.950 kg of synthetic electrolyte were added to the crucible. This weicjht of molten electrolyte should have resulted in an electrolyte pool 13 cm deep.

The furnace was heated according to the heating schedule shown in Figure 3.4. Slow heating was used to minimize the chances for thermal cracking of the Al_2O_3 liner. At no time did the furnace heating rate exceed 50°C per hour. Initially, the furnace temperature was set to 1010°C to melt the electrolyte, and was then lowered to the operating temperature, 970°C. Once the electrolyte was molten, a bath sample was collected for ratio analysis. The bath ratio was raised to 1.35 by the addition of NaF.

TABLE 3.3. Impurities of Test Constituents

	%Fe	%Cu	%Ni
Aluminum Metal	0.365	0.0018	0.0039
Alumina	0.0044	t0.0001	0.0006
Electrolyte	0.063	0.0031	0.0001
Graphite Crucible	0.0409	<0.0001	0.0017
Pilot Cell Electrolyte	0.019	0.0004	0.0007

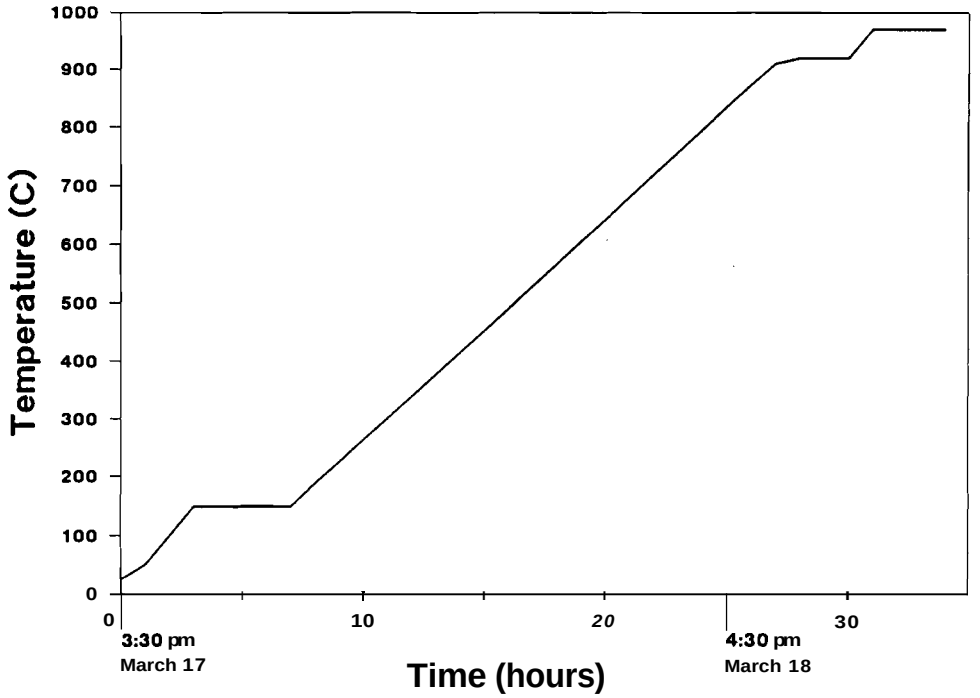

.FIGURE 3.4. Furnace Preheat Cycle

3.2.4 Inert Anode Preheat and Transfer

During the time the graphite anode was being used to break in the new cell, the inert anode was heated in air in a box furnace. The temperature in the furnace was manually adjusted so that the temperature increased at or less than 50°C/h. When transferred to the electrolysis cell, the cermet anode temperature was 937°C.

Finite element analyses and previous experience with a large cermet anode suggested that the transfer must be done rapidly and with a minimum exposure to ambient temperatures. So that thermal shock could be minimized, a metal shroud was constructed from two coaxial metal tubes. The inner tube was welded to the outer tube using a donut-shaped plate. The annulus between the tubes was filled with insulating batting. This arrangement was split length-wise to make a clamshell-type device. With the clamshell closed, the inert anode was hoisted from the furnace into the insulated can. The can and anode were rapidly carried to the electrolysis cell where the anode was lowered into the hot zone of the furnace. The clamshell can was removed, and

the electrical connections and support connections were established. No evidence was found that this transfer had caused any cracks to form in the anode, although a crack was noted some time into the electrolysis experiment.

3.2.5 Signal Monitoring

Several types of sensor and instrument combinations were used to monitor current and voltage signals for online and post-test evaluations conducted by PNL. The data for PNL work included digital current and voltage, analog data obtained with strip chart recorders, reference anode data, and data for current density calculations.

Digital Signal Data

Digital signal data for DSA, obtained during the test, consisted of the following:

A. cell current
B. cell voltage from top of working anode stem to cathode
C. cell voltage from inner surface of working anode to cathode
D. voltage from reference anode to cathode.

The measurements were made using the instruments and sensors assembly shown in Figure 3.5. An IBM AT® PC was used with the Rapid Systems, Inc., Seattle, Washington, R360 Real Time Spectrum Analyzer software for data acquisition, control, and storage. The Spectrum Analyzer consisted of an R300 Digital Signal Processing (DSP) interface board and a 4X4 Digital Oscilloscope Peripheral. Inputs to the 4X4 included the cell current (A) collected across a transducer in the working anode stem; the cell voltage from the top of the working anode step to the cathode (B); the cell voltage from the inner surface of the working anode to the cathode (C); and the voltage from the reference anode to the cathode (D).

The reference anode was an electrode with the same composition as the prototype anode but of smaller dimensions, with a length of 6.4 cm and a diameter of 1.9 cm. This electrode was used as a reference against which the. potential of the prototype anode was measured. Key to the success of this

---

® International Business Machines, Armonk, New York.

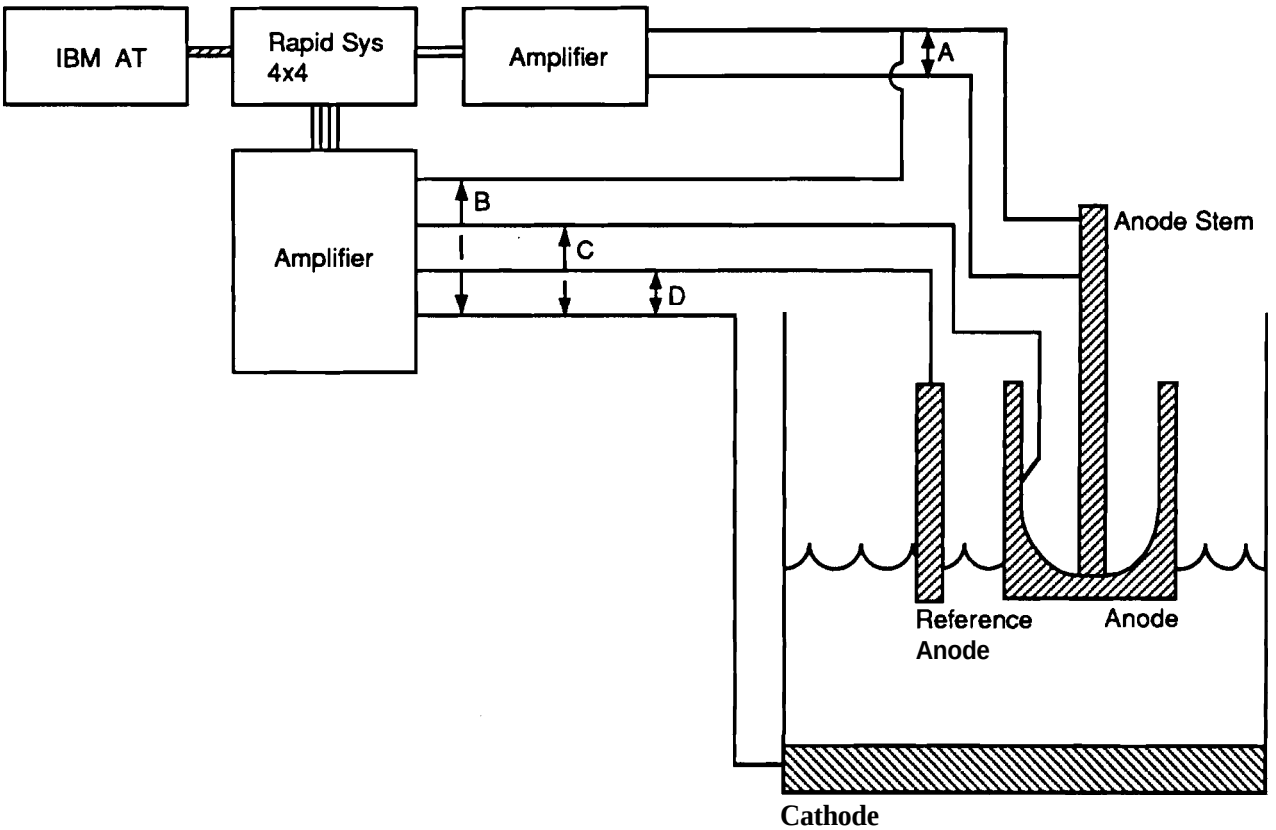

FIGURE 3.5. Sensor and Instrument Assembly for Digital Signal Measurement

procedure was the stability of the reference anode. To keep it from corroding, a small anodic current was passed through it throughout the test.

The data were collected in the form of sets of digital signals of items A through D recorded at selected times during the test. Each set of data consisted of 2048 sequential signals collected over a period of 0.4 s (5 kHz sampling frequency). During this short period of data collection, the cell operating conditions, including temperature and bath composition, were assumed to be constant.

The digital signal data were stored as files on 1.2 MB magnetic disks. The cell operating conditions at the approximate times each set of data were collected are given for these files in Table 3.4. The digital signal data were forwarded for analysis to Dr. C. L. Nikias on May 26, 1989.

TABLE 3.4. Descriptions of Conditions at Data Collection Times

File	Date	Time	Temp.	Volts	Amps	B.R.	$\%Al_2O_3$
NIKRSAT 6-9	3/20/89	22.35	973°C	3.69	120.6	1.45	8.03
NIKRSA 20-22	3/21	10.38	992	3.50	120.7	1.35	7
NIKRSA 23-25	3/21	17.01	980	3.45	120.7	1.34	7.91
NIKRSA 27-29	3/21	19.55	979	3.65	139.5	1.32	7.59
NIKRSA 30-32	3/22	11.29	972	3.57	121.5	1.28	7.53
NIKRSA 3A-3B	3/22	19.18	981	3.52	120.5	1.27	7.55
NIKRSA37	3/22	22.30	967	3.24	83.0	1.26	8.09
NIKRSA 40-42	3/23	8.24	989	3.53	120.4	1.26	7.77
NIKRSA 43-45	3/23	10.27	985	2.96	120.5	1.26	9.43
NIKRSA 46-48	3/23	14.50	989	3.68	120.4	1.26	9.11
NIKRSA 49-48	3/23	19.15	---	---	---	1.32	8.46
NIKRSA 50-52	3/24	10.15	---	3.68	120.6	1.28	8.68
NIKRSA 56-58	3/24	13.40	982	3.75	120.4	---	7.93
NIKRSA 59-58	3/24	18.50	987	3.25	119.5	1.29	8.75
NIKRSA 5Y-5W	3/24	19.50	983	3.89	---	---	7.6
NIKRSA 5E-5G	3/24	22.45	974	3.89	119.4	---	7.83
NIKRSA 6A-6B	3/24	23.45	---	3.85	119.4	1.26	8.93
NIKRSA 61-62	3/24	8.12	987	3.95	119.7	---	8.01
NIKRSA	3/24	9.16	952	---	---	---	8.18

Other Digital Data

In addition to data collected for Dr. Nikias, other digital signal data were analyzed in' various ways to determine, in particular, the variations of current and voltage over longer time durations than those appropriate for standard DSA. The same instrumentation described above was used to collect these additional digital signal data. Most of these additional data showed little, if any, variation with time, and therefore resembled the DC current.

Reference Electrode Data

Four reference electrodes were constructed using the method of Burgman, Leistra, and Sides (1986). Only one of the electrodes was used to measure the voltage drops within the cell. Although some voltage measurements were made, there was sufficient uncertainty in the position of the probe with respect to the anode and cathode that the numbers have only marginal meaning. The single point voltages made with the reference electrode were +450 mV with respect to the cathode and -278 mV with respect to the anode.

Analog Data

Strip chart recorders were used to monitor certain cell operating conditions:

R1. cell voltage
R2. voltage from working anode to reference anode
R3. current through the reference anode
R4. root mean square (RMS) voltage.

The recorders were connected to the prototype anode and test cell as shown in Figure 3.6.

3.3 CHEMICAL ANALYSES

3.3.1 Bath Ratio

The bath ratio (i.e., the weight ratio of NaF/AlF_3) was determined for electrolyte samples. This ratio was determined by grinding a sample of electrolyte to a fine powder (<100 mesh), weighing out 8 g, melting it in a platinum crucible at 1100°C, and titrating to a phenolphthalein end point using "single point ratio tablets." Single point ratio tablets contain 28 mg

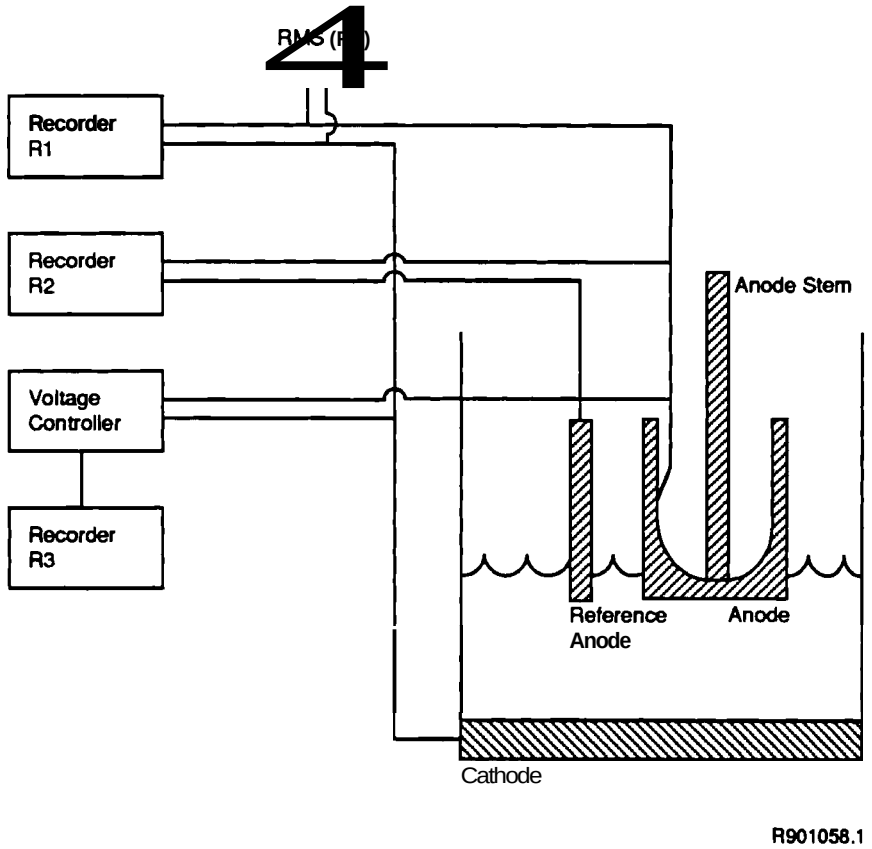

FIGURE 3.6. Strip Chart Recorder Arrangement

NaF and 22 mg NaCl. These tablets were added one or more at a time to the molten sample of the electrolyte, which was then stirred with a platinum wire. After complete mixing, a bead of frozen electrolyte was formed on the platinum wire by first cooling the wire in air and dipping it in the molten electrolyte three times with cooling between each time. The bead of frozen electrolyte was then briefly cooled in air and dipped into distilled water. A couple of drops of phenolphthalein solution were then added to the moist bead. A faint pink color on the bead after adding the phenolphthalein solution signified that the end point had been reached. The bath ratio was obtained from a table that gave the bath ratio corresponding to the number of tablets added to an 8-g sample. The values in this table were based on the equation:

$$R = \frac{1.50 \cdot C - A}{1.0 \cdot C + A} \qquad (1)$$

where $A = W_1/W_2$

W_1 = the mass of NaF added to the sample (need to take the purity of the NaF into account)

W_2 = the mass of the electrolyte sample (8 g in this case)

C = the fraction of NaF + the fraction of AlF_3 in a standard electrolyte (0.84 in this case).

3.3.2 Alumina Analyses

Alumina analyses were performed on many of the electrolyte samples to determine the feed rate for the cell. Dissolved alumina in the cryolite was determined gravimetrically by dissolving 1 g of finely powdered electrolyte in 50 mL of a saturated $AlCl_3$ solution (30 mass%). This solution was allowed to boil for 10 min and then quickly filtered through Whatman No. 4 ashless filter paper containing a small amount of filter aid. After the solution had been filtered, the solid and filter paper were extensively washed with hot (nearly boiling) demineralized water until the filtrate tested neutral to litmus and yielded no precipitate when tested with 0.1 M $AgNO_3$. The washed filter paper containing the residual Al_2O_3 was ashed and then fired at 1000°C for a minimum of 15 min in a tared and covered platinum crucible. After firing, the residual material was allowed to cool in a desiccator for 15 min and weighed.

3.3.3 Trace Element Analyses

One-gram samples of finely ground electrolyte were dissolved in boiling 6 M HCl. This solution was diluted to 100 mL with demineralized water, and the trace elements were determined using an inductively coupled plasma spectrometer (ICP). At PNL, any material that remained undissolved was filtered from the solution and the solids fused with Na_2O_2 in a Zr crucible. This fusate was then dissolved in HCl and the resulting solution quantified using the ICP.

Aluminum metal samples were cleaned using a combination of NaOH, HCl, and HNO_3 in succession. A sample weighing approximately 1 g was weighed and dissolved in about 50 mL of 6 M HCl to which about 5 mL of concentrated HNO_3

had been added. The HNO_3 was needed because any impurities in the metal tended not to dissolve in the HCl. The resulting solution was diluted with demineralized water to 100 mL and was quantified using the ICP. Any undissolved material remaining after acid dissolution was filtered from the solution and fused with Na_2O_2 for subsequent quantification in the ICP.

3.3.4 Calcium Content of the Electrolyte

The calcium content of the electrolyte was determined for all of the electrolyte samples. Calcium was determined in the electrolyte samples at PNL using the ICP as described above, but was determined using a titration method at Reynolds Metals Company. In the titration method, a 1-g sample was dissolved in 6 M HCl and boiled for 10 min. The pH was adjusted to about 13 with 6 M KOH. A small amount of calcium indicator was added to the solution, and the solution was titrated to a green end point with a solution of disodium ethylenediaminetetraacetic acid (EDTA; 17.1 g/L).

3.3.5 Impurity Resulting from Dissolution of Reference Electrodes

Two of the reference anodes dropped off of the electrical connection and were lost in the molten Al pool. The mass of these anodes (-30 g each) was insignificant relative to the mass of the Al in the bottom of the cell. If the reference anodes totally dissolved, the maximum contribution to the impurity content would be on the order of 0.5%.

3.3.6 Chemical Composition of the Anode

Weighed portions (approximately 1 g) of anode materials, including the oxidized portions, were dissolved in approximately 30 mL of hot concentrated HCl. Dissolution required several hours to several days of heating before all of the ferrite and NiO material dissolved. Approximately 3 mL of concentrated HNO, were added to the cooled HCl solution to ensure that all of the Cu had been dissolved. This solution was then diluted to 100 mL with demineralized water. The dissolved constituents were quantified using the ICP. Any undissolved material remaining after acid dissolution was filtered from the solution and fused with Na_2O_2 for subsequent quantification in the ICP.

3.4 SOLID-STATE ANALYSES

3.4.1 Scanning Electron Microscopic Analyses

Samples of the prototype anode were taken after the anode had been photographed and cut in half. Samples for optical metallography and SEM were taken from the bottom, side at the melt line, and top of the rim. These samples were mounted in a thermoset epoxy and polished. After examination under an optical microscope, the samples were vapor-coated with an electrically conducting layer of carbon and mounted in the SEM. A sample of the prototype anode before it was used and a sample of a "standard" anode material that had been made much earlier were examined along with the vapor-coated samples. The SEM was operated in the quantitative mode to get an accurate picture of the changes that occurred during the test of the prototype anode and, hopefully, to determine any changes in the phase composition during use of the prototype anode. The system was calibrated using a Cu metal standard.

3.4.2 X-Ray Diffraction Analyses

Samples from the oxidized layer on the working surface of the anode below the surface of the electrolyte and the oxidized material on the anode rim were submitted for x-ray diffraction (XRD) analyses. These samples were first ground to a fine powder. Samples that had been mounted for metallography and SEM were also examined using XRD. In this method, approximately 1.3 mm x 25 mm of the surface could be examined, and an estimate of any phase changes with position could be obtained. This information was useful for interpreting the SEM results.

As will be discussed in Section 4.3, the composition of the Cu/Ni alloy that made up the metallic portion of the cermet changed during the test. Diffraction patterns for three Cu/Ni alloys were obtained from the Powder Diffraction File (PDF 1986), and three of the strongest diffraction peaks were selected for comparison. Figure 3.7 summarizes the results from this comparison. Since the position of the diffraction peaks is a linear function of the alloy composition over the range 100% Cu to 100% Ni, the straight

lines shown in Figure 3.7 or the least squares fit linear equation can be used to determine the composition of Cu/Ni alloy in the cermet. A Cu/Ni composition was obtained by comparing each of three Cu peaks. These three compositions were then averaged.

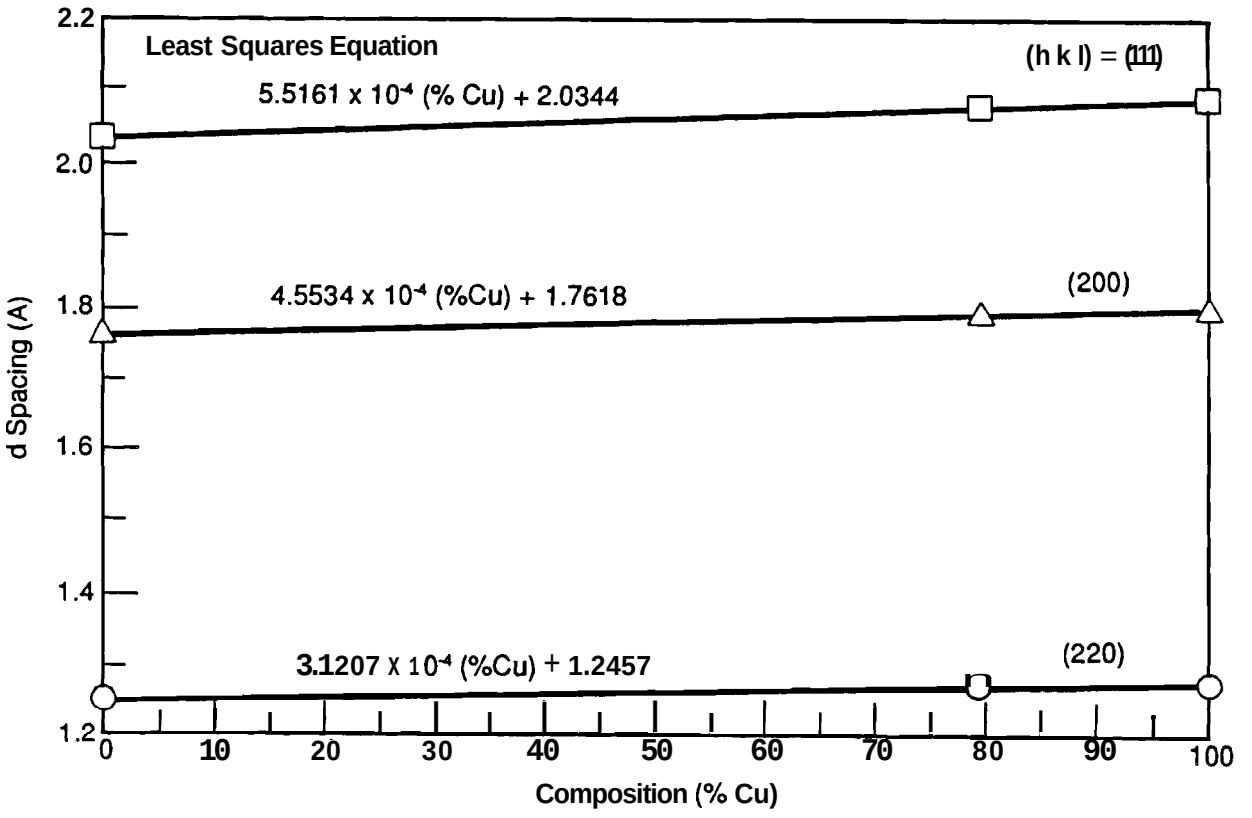

FIGURE 3.7. Composition of Cu/Ni Alloy by XRD Line Position

4.0 RESULTS AND DISCUSSION

Results from the large-scale experiment, including cell operation, anode characteristics, and signal monitoring data, are discussed in this section.

4.1 CELL OPERATION

The effects of operating the electrolysis cell during the 113-h experiment are discussed under the following headings: electrical results, electrolyte chemistry and temperature, Al metal purity, and cell mass balance.

4.1.1 Electrical Results

A log of the voltage and amperage for the cell during the time the graphite anode was used is shown in Figure 4.1. In this figure, the current scans are shown as decreases in both voltage and amperage. An anode effect during which the voltage increased is shown at 22.16 h. The results from the second of these current scans are shown in Figure 4.2; the data from all of the current scans are given in Table A.l in the Appendix. By extrapolation to zero current, the back emf of the cell with the graphite anode is 1.84 V (Figure 4.2). The average of the last three determinations of the back emfs where the anode-to-cathode distances were about the same is 1.92 ± 0.07 V.

A log of the voltage and amperage for the cell during the time the inert anode was being used is shown in Figure 4.3, along with current scans. The results from the current scan at 4.4 h are shown in Figure 4.4. By extrapolation to zero current, the back emf of the cell with the inert anode is 2.25 V (Figure 4.4). The average back emf for the last nine current scans is 2.23 ± 0.02 V. The theoretical decomposition voltage for an oxygen-evolving anode is 2.22 V. The low offset between the observed and calculated voltages may be a result of a low overvoltage, the lack of anode polarization, or a contribution to the electrical character from anode corrosion.

Figure 4.3 also shows the control strategy used to reestablish the proposed protective film on the anode (Strachan et al. 1989). Anode instability is indicated when the anode voltage signals begin to show spikes. When this spiking occurs, the current to the cell is reduced in order to allow the film to mend. When the film is mended, the current is increased slightly. If the

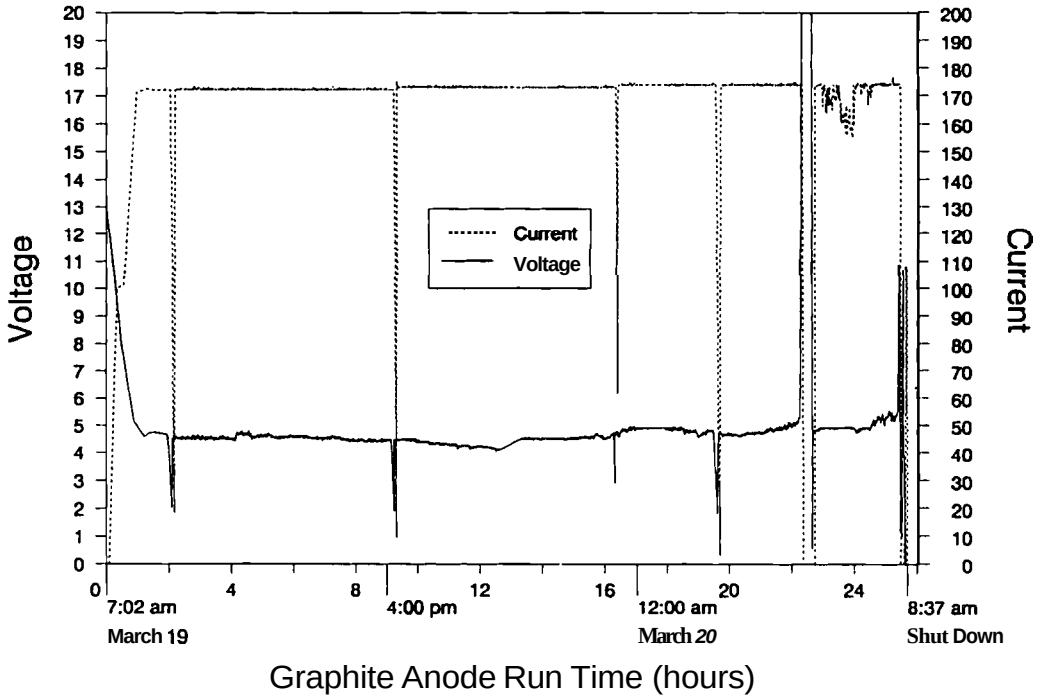

FIGURE 4.1. Cell Current and Voltage During Graphite Anode Run

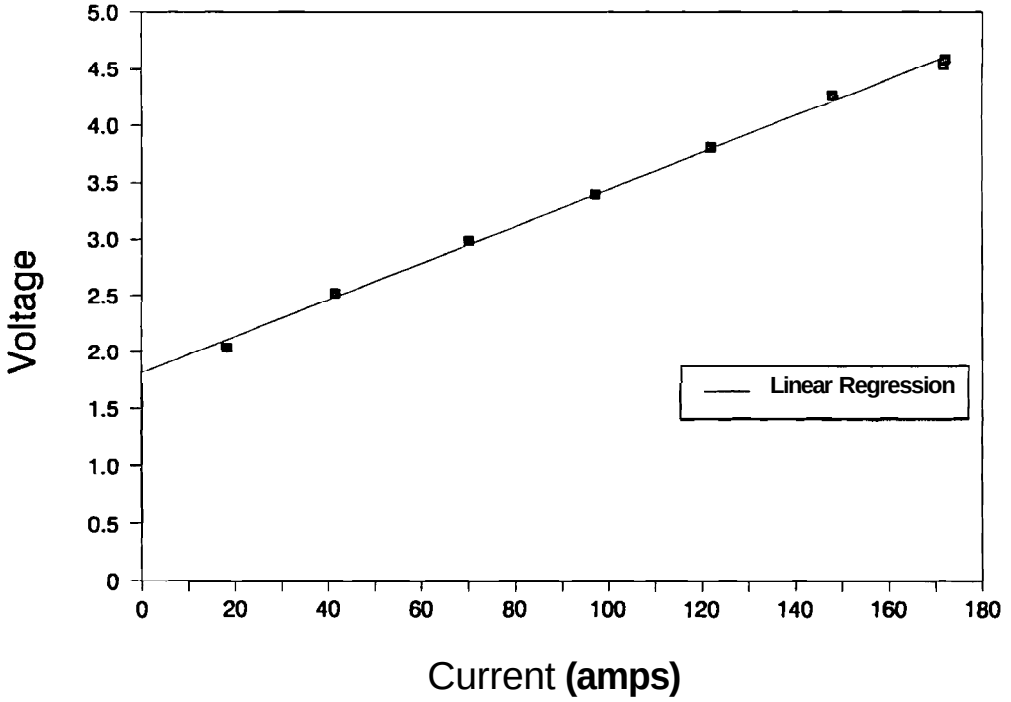

FIGURE 4.2. Current Scan of Graphite Anode Electrolysis

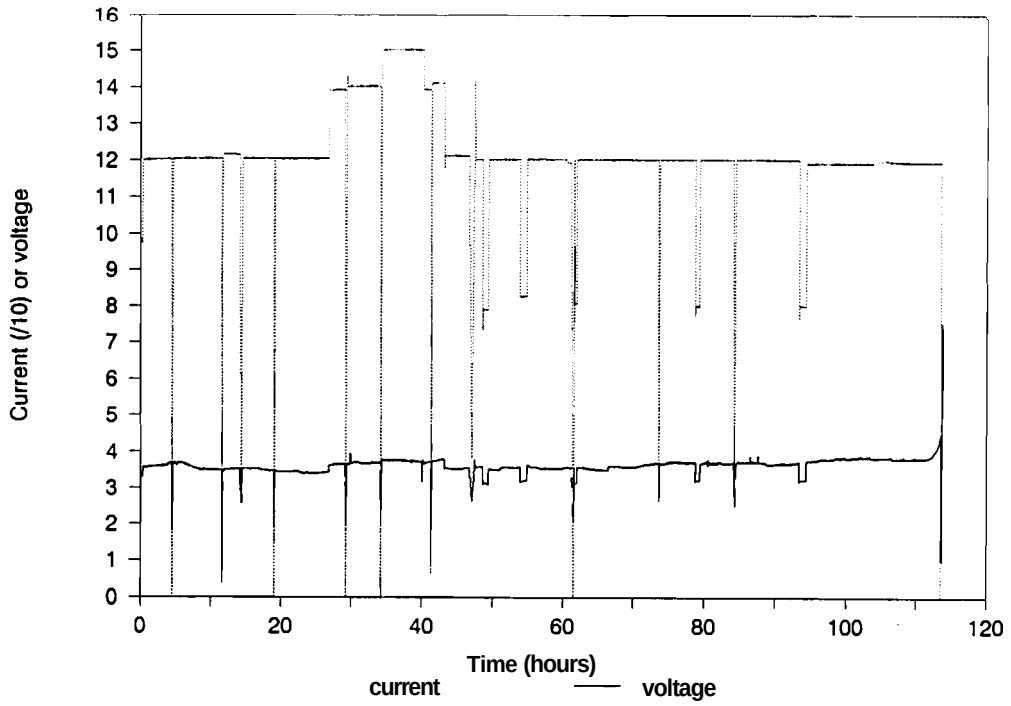

FIGURE 4.3. **Current and Voltage During Inert Electrode Run**

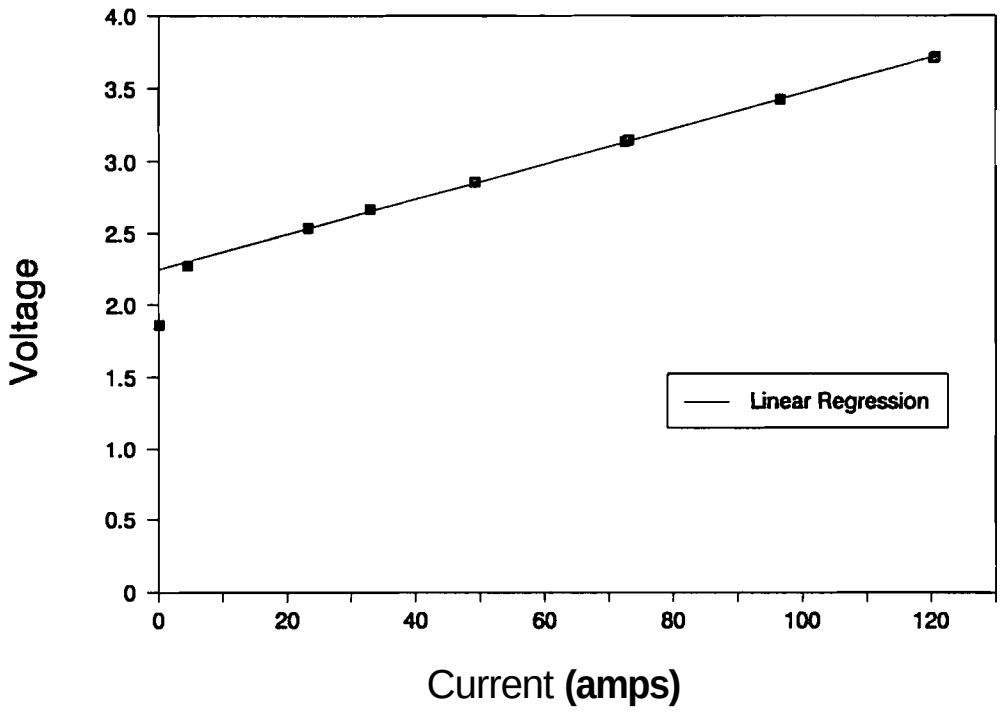

FIGURE 4.4. **Current Scan at 4.4 h of Inert Anode Electrolysis**

TABLE 4.1. Cell Voltage Breakdown for Graphite Anode (Cell Current = 172.0 A)

System Voltage	4.75V
Bus Drop	0.73
Cell Voltage	4.02
Anode Drop	0.17
Decomposition Voltage	1.19
Bath Drop	2.19
Cathode Drop	0.24
Polarization Voltage	0.23

TABLE 4.2. Cell Voltage Breakdown for Ferrite Anode (Time = 7.0 h; Cell Current = 120.62 A)

System Voltage	3.69
Bus Drop	0.46
Cell Voltage	3.23
Anode Drop	0.065
Decomposition Voltage	2.22
Bath Drop	0.635
Cathode Drop	0.28
Polarization Voltage	0.03

3.8 cm. An electrolyte voltage drop of 0.635 V was calculated assuming that the voltage can be calculated using a cylindrical geometry, which does not take the anode bottom into account, and assuming a value of 2.40 $ohm^{-1}cm^{-1}$ for the electrolyte conductivity.

While the voltage values may not be absolute, a very small polarization voltage is indicated in Table 4.2 for an inert, oxygen-evolving anode. This same observation was obtained from the data summarized in Figure 4.4.

4.1.2 Electrolyte Chemistry and Temperature

The temperature, bath ratio, Al_2O_3 content, and trace element content were measured as a function of time. These data are shown in Figures 4.6 through 4.9.

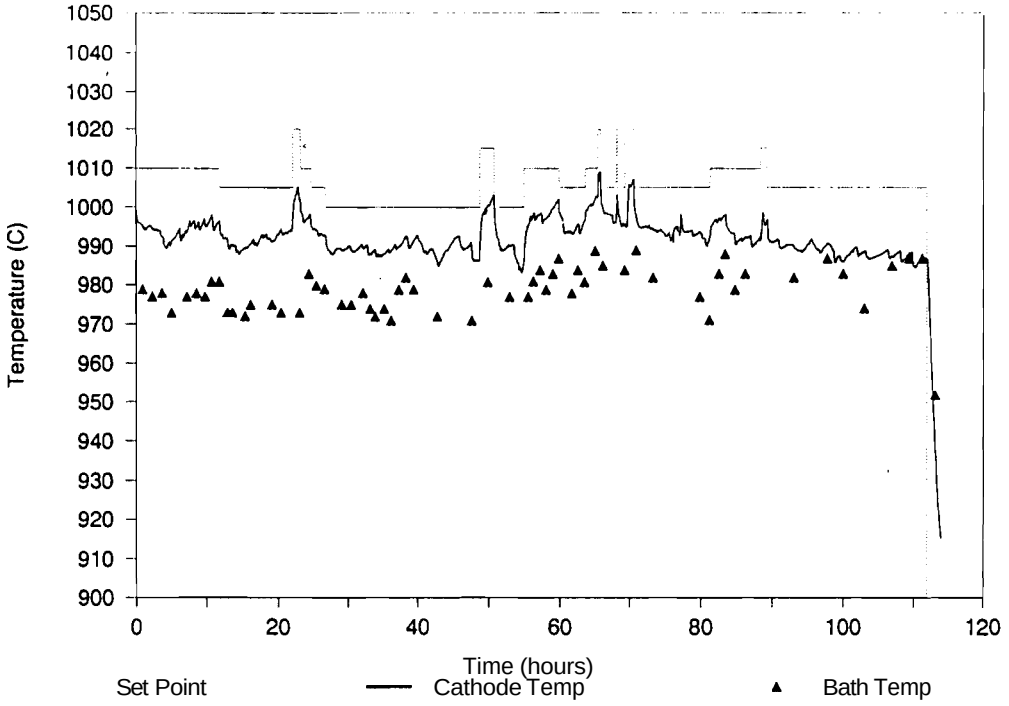

FIGURE 4.6. Temperature History for the Prototype Anode Test Cell

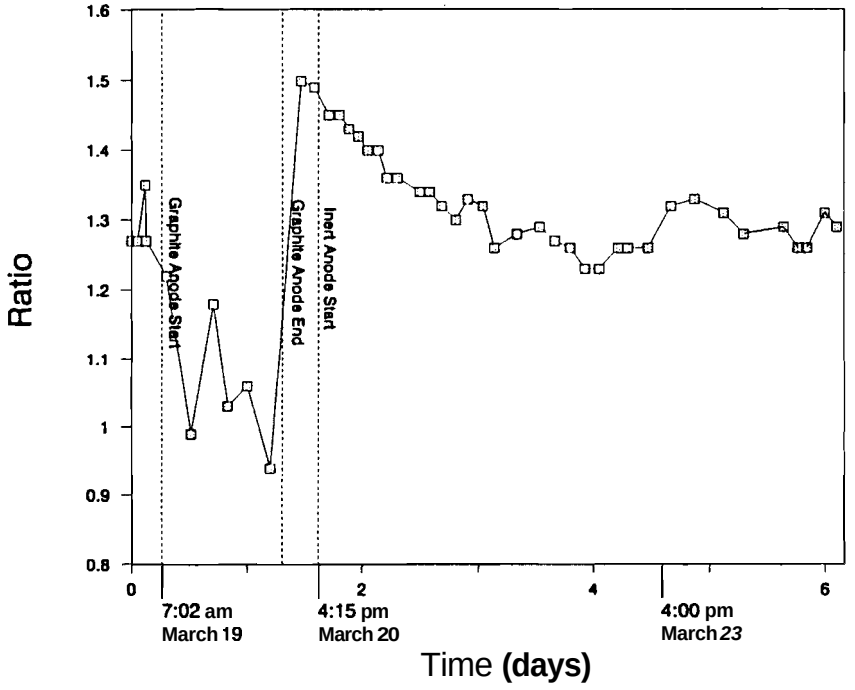

FIGURE 4.7. Summary of the Bath Ratios for the Electrolyte in the Prototype Anode Test

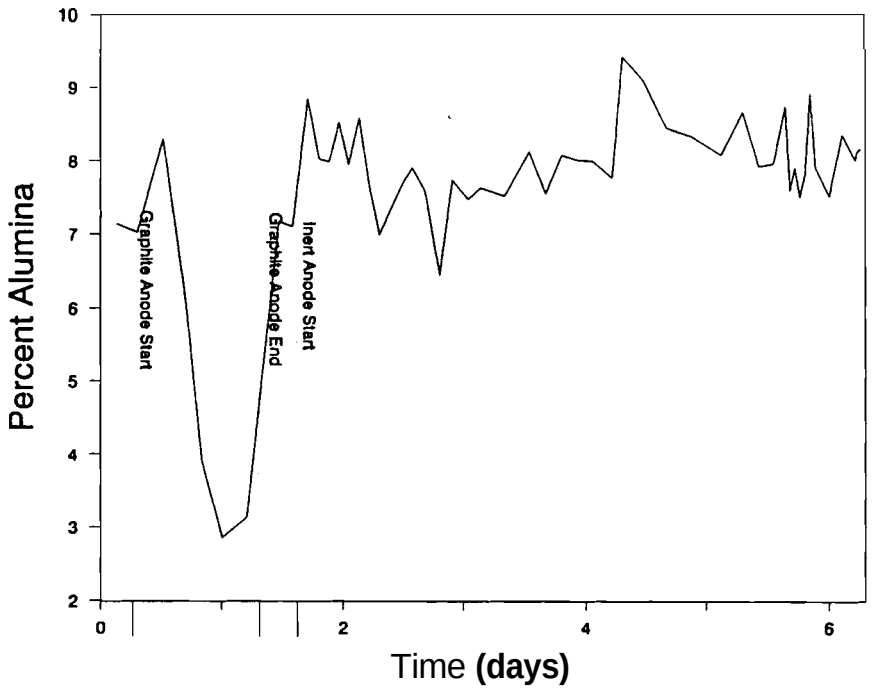

FIGURE 4.8. Results from Analyses of the Dissolved Al_2O_3 in the Electrolyte Used in the Prototype Anode Test

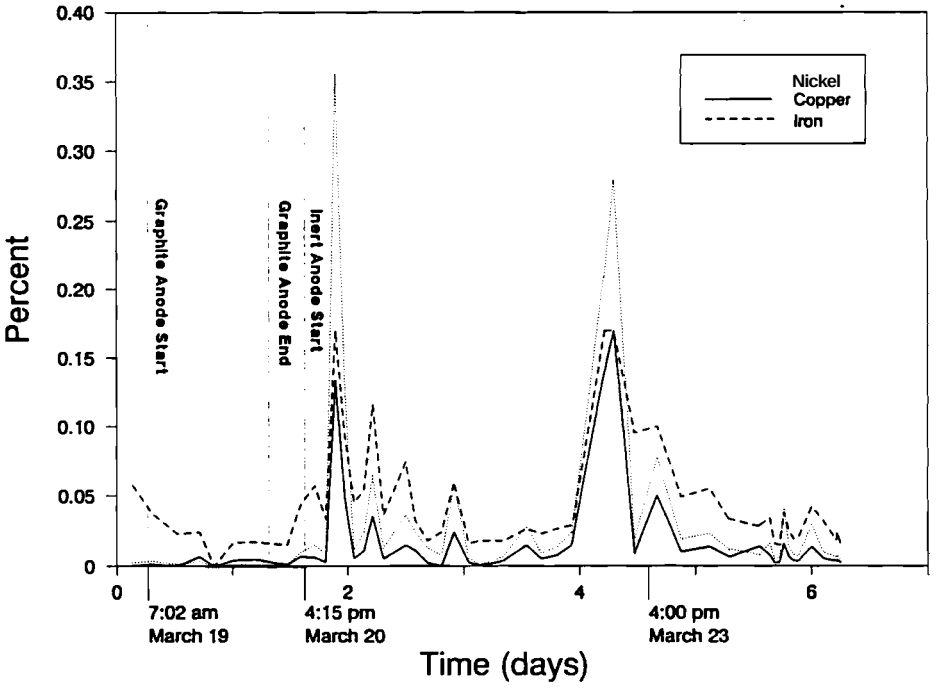

FIGURE 4.9. Results from the Analyses of Cu, Fe, and Ni in the Electrolyte Used in the Prototype Anode Test

The furnace set point, cathode temperature, and electrolyte temperature are presented in Figure 4.6. The cathode temperature closely matches the furnace set point with only a small lag time. The electrolyte temperature averages about 10°C lower than the cathode temperature. During the graphite anode portion of the test, the set point was lowered to reach an operating temperature of 970°C in the electrolyte. At the end of the graphite anode portion of the test, the set point was raised to 1010°C to facilitate the melting of electrolyte additions. Electrolyte lost during the graphite anode portion of the test had to be replenished before the start of the inert anode portion of the test.

During the cermet anode portion of the test, the electrolyte temperature was 980°C for the first 12 h of operation, and then decreased after the furnace set point was lowered by 5°C to bring the operating temperature to 975°C. The cathode temperature was reasonably stable during this period except when electrolyte was added to the cell, which typically caused the temperature to decrease 2°C to 5°C. Bath additions were being made during this period to maintain the anode immersion depth at 5 cm. The type and amount of additions can be found in the Appendix (Table A.2). The temperature was held constant except for brief periods where the set point was raised by 10°C to 15°C to help melt bath additions that had frozen on the anode and cell liner. At 55 h into the inert anode portion of the test, the set point was raised 10°C to offset the cooling effect of an increased argon flow. Near the 112-h mark of the inert anode portion of the test, the furnace thermocouple failed. This condition caused the furnace controller to shut down, After approximately 1 h, the faulty thermocouple was discovered and replaced. However, the controller could not be restarted because of a faulty furnace "Fail-safe" switch. At this point the anode was raised out of the electrolyte and allowed to cool with the furnace.

In Figure 4.7, the variability in the bath ratio for the test is shown. During the graphite anode portion of the test; the bath ratio decreased steadily despite additions of NaF. In the 3 h between the graphite portion of the test and the cermet portion, commercial electrolyte and NaF were added to correct the low ratio. These additions were made assuming the commercial electrolyte had a ratio of 1.35; it was later discovered to have a 1.45

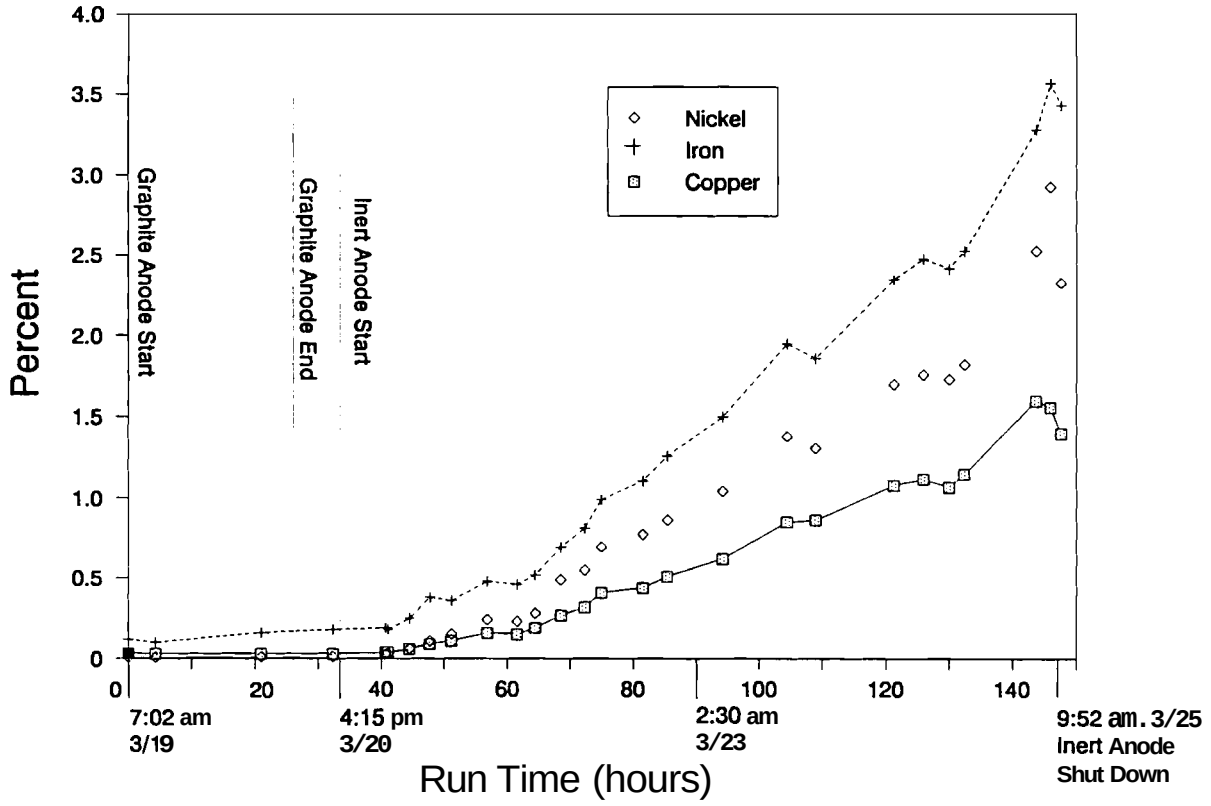

FIGURE 4.10. Copper, Iron, and Nickel Concentrations in the Metal During the Prototype Anode Test

The data of Goodes and Algie (1989) suggest that significant quantities of Cu, Ni, and Fe should have volatilized.

Although a plot of the impurity concentrations in the Al metal shows the rate at which impurity concentrations were increasing in the Al metal (Figure 4.10), it is perhaps more instructive to look at the ratios of the impurities and compare these ratios with the ratios in the original cermet. In Figure 4.11, the observed ratios of impurity metals in the Al metal divided by the corresponding ratio in the cermet are plotted against the time of the test. For the graphite portion of the test, the comparison is not valid. The comparison can be made from the time the cermet anode was placed in the cell at about 40 h when the ratios began to change. The Cu/Ni ratio was initially about 16 and decreased rapidly to a steady-state value that was greater than the ideal of 1.0. The initially high value occurred because the initial Ni concentrations in the system were very low but were eventually

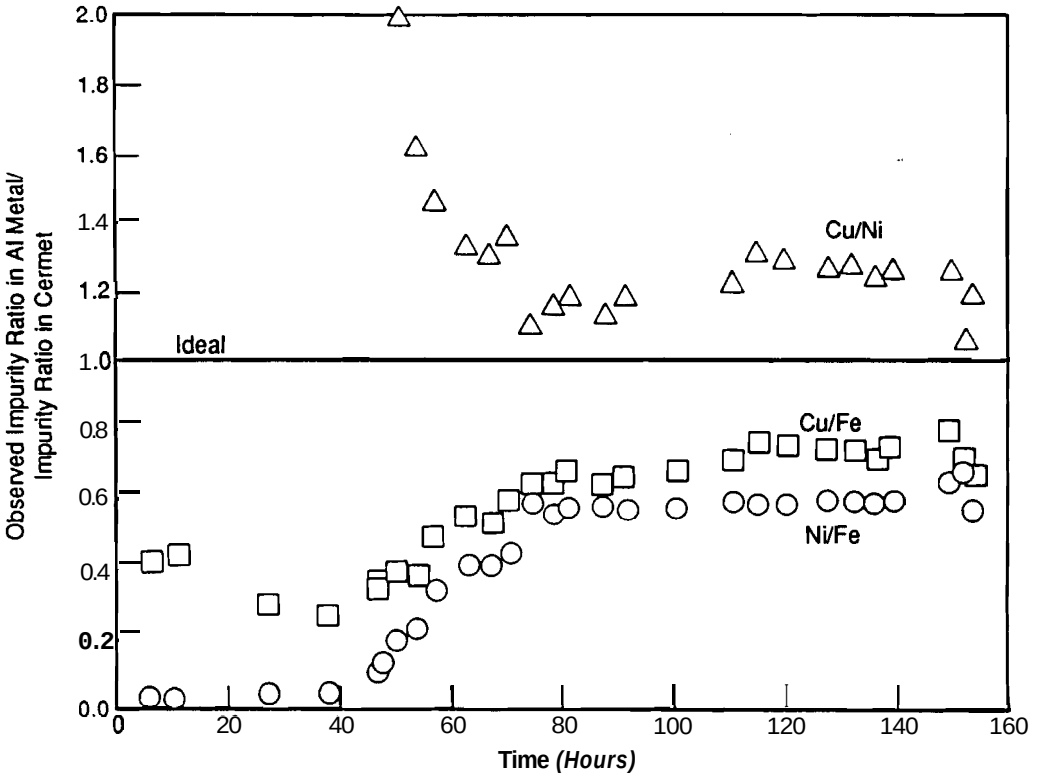

FIGURE 4.11. Comparison of Observed Impurity Ratio in Al Metal with Impurity Ratio in Cermet

dominated by the contribution from the anode corrosion. The Cu/Fe and Ni/Fe ratios increased during the cermet portion of the test to steady-state values below the ideal value of 1.0. Correcting for the contribution to the impurity concentration from the Cu, Fe, and Ni contents of the electrolyte equalizes the Cu/Fe and Ni/Fe ratios at a value near 0.75, whereas the Cu/Ni ratio approaches 1.0. Thus, it would appear that the Cu and Ni were selectively, but equally, volatilized while, relative to the Cu and Ni, the Fe remained behind and concentrated in the metal phase. Hence, the corrected steady-state ratio for Cu/Ni approaches 1.0, whereas the Cu/Fe and Ni/Fe ratios approach a value less than 1.0.

4.1.4 Cell Mass Balance

During the test, an accounting was maintained for all materials added or removed from the cell. The mass balance for the electrolyte may be found in the Appendix (Table A.1.1). A total of 34.119 kg of electrolyte and

additives were used during the 113-h period with the cermet anode and the 24-h period with the graphite anode. A total of 14.232 kg of material either were collected by sampling, remained in the cell, adhered to various parts of the test equipment, or were accounted for by other means. The remainder, about 20 kg of electrolyte, was either lost to the cathode or, most likely, volatilized.

An inventory of the metal was also maintained during the test (Appendix, Table A.2). A total of 1.911 kg of metal was produced during the entire test sequence. For the 24 h of electrolysis with the graphite anode, the current efficiency was estimated at 79.0% or 124 g of Al. The remaining metal was generated during the cermet anode portion of the test and equates to a current efficiency of 38.8%. No correction for the dissolved impurities was made because the error in the current efficiency calculation was already high. A number of factors could have contributed to the low current efficiency such as cell design and high operating temperature.

4.2 ANODE CHARACTERIZATION

After 113 h of electrolysis, the anode was raised from the electrolyte, but remained in the hot zone of the cell and allowed to cool with the furnace and the cell. When the anode was removed from the cell, four cracks were observed (Figure 4.12). While one of these cracks was seen during the test, the others were not. For the most part, the cracks appeared to have resulted from the mismatch in the coefficients of thermal expansion between the cermet and the Ni/Cu alloy used to connect the Ni rod to the anode. Laboratory-scale anodes with cracks have successfully been tested, i.e., suffered little corrosion (Marschman 1989).

The anode was cut in half down the axis of symmetry (Figure 4.13). Evidence of extensive corrosion could be seen with the unaided eye. A halo of copper-colored material was observed to the anode interior of all outer surfaces of the anode. The upper parts of the anode or rim were severely oxidized to the point that some spalling undoubtedly occurred, which was surprising since extensive corrosion was not seen on the upper rims of the

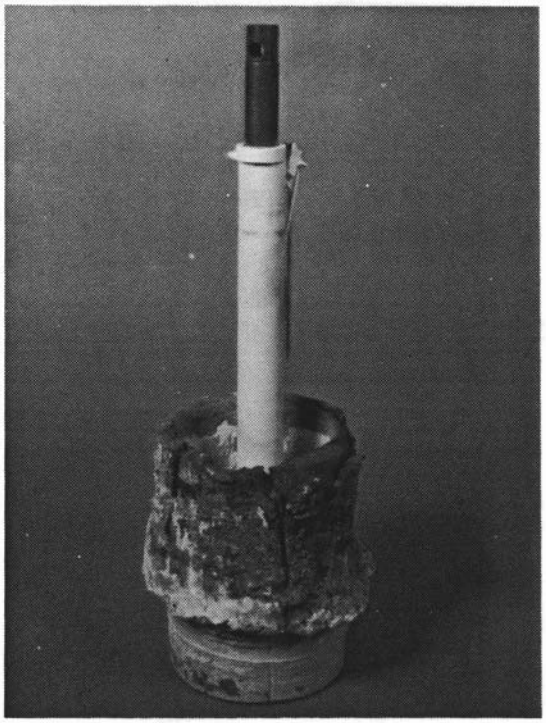

FIGURE 4.12a. Prototype Anode After Testing

FIGURE 4.12b. Bottom Face of the Prototype Anode Showing the Cracks That Developed During the Test

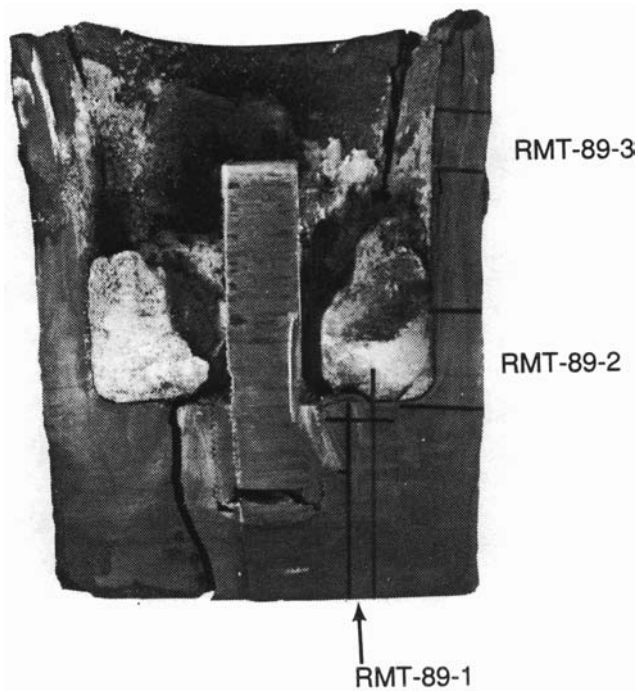

FIGURE 4.13. Photograph Showing the Used Prototype Anode in Cross Section and the Places at Which Samples Were Taken for Solid-State Analyses

laboratory-scale anodes. A rind of dark, oxidized material, approximately 3 mm thick, was found on the surface that had been immersed in the electrolyte.

The oxidized portion of the anode below the electrolyte was uniformly thick except near the melt-electrode-air interface, suggesting uniform corrosion and current density. Using the dimensions indicated by corrosion and the average current through the anode, an average current density of 0.63 A/cm^2 was calculated.

Three samples were cut from the anode for metallographic and SEM analyses. One sample was cut from the upper rim of the anode; one sample was cut from the area of the melt line; and one sample was cut from the bottom. These sample locations are marked in Figure 4.13. Additional samples were taken from these and other areas for x-ray and chemical analyses. The results from these analyses are reported below.

4.2.1 Anode Rim

Oxidation was most prevalent in the rim area. Portions of the rim were oxidized completely (Figure 4.14), and a copper-colored halo was observed near the oxidized zone but within the remaining cermet (not seen in the photomicrograph because of the lack of contrast for that zone). Results from the x-ray analyses of material well within the oxidized zones showed that the NiO and $NiFe_2O_4$ phases were still present, but the Cu had been oxidized to CuO (Figure 4.15). There also appeared to be an increase in the intensity of the NiO lines, indicating a possible increase in the NiO content relative to the starting material. Although the remaining cermet portion of the anode rim did not physically appear to be oxidized, the relative peaks of the ferrite and NiO portions in the XRD pattern indicated an increase in the NiO content of the cermet. Comparison of the positions of three diffraction

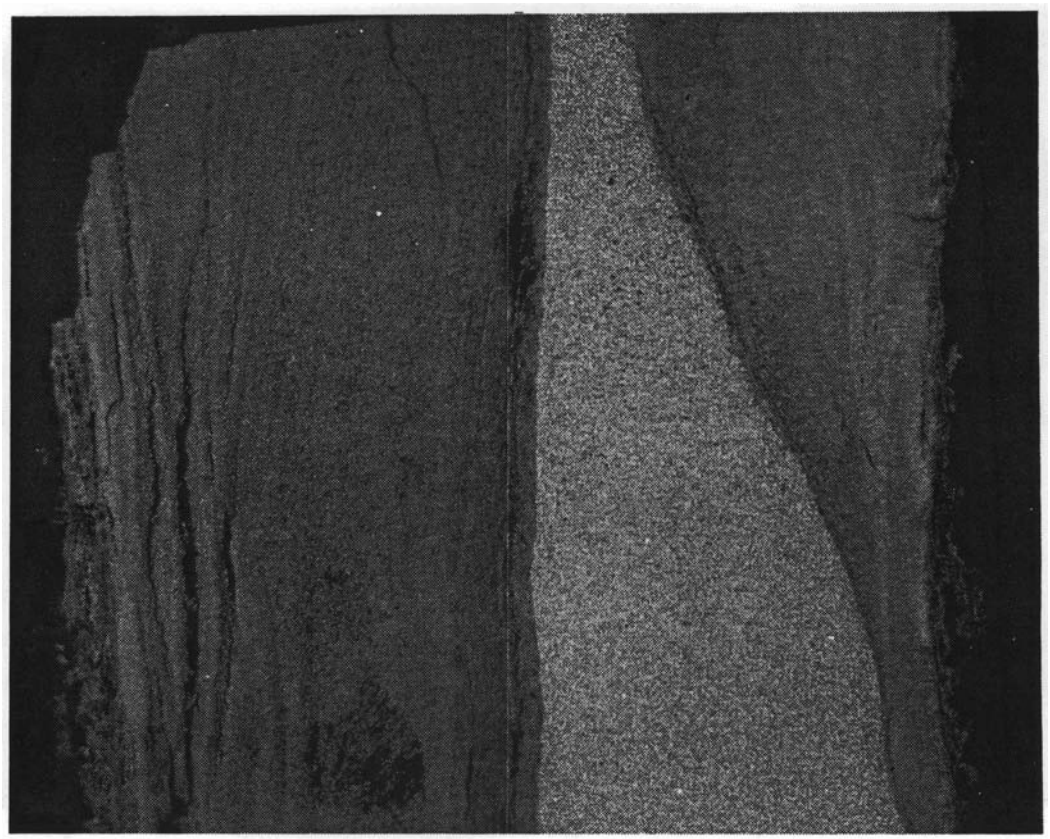

FIGURE 4.14. Upper Portion of the Prototype Anode Rim Showing the Degree of Oxidation. The left side of the sample was the inside of the anode.

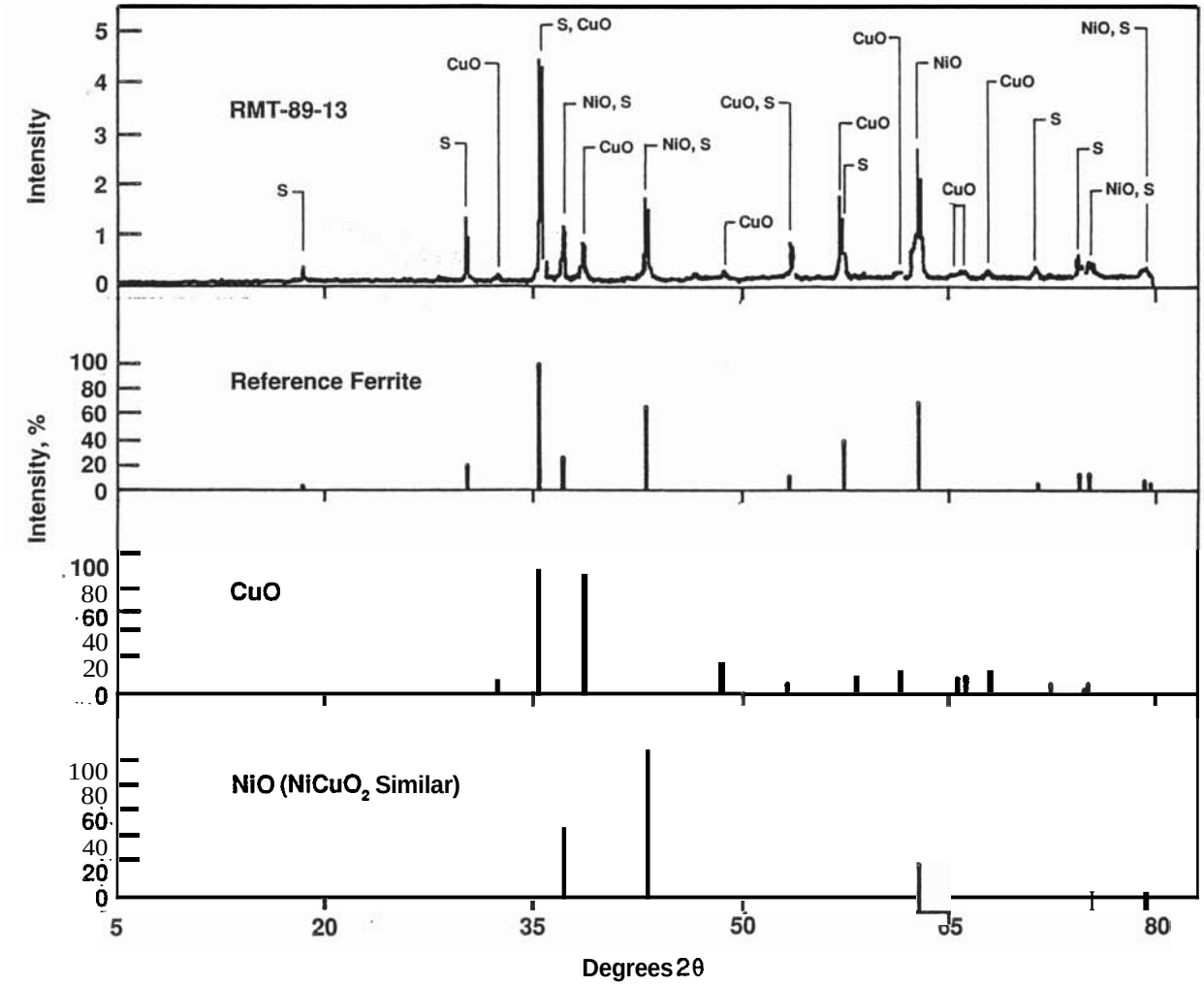

FIGURE 4.15. Results from the XRD Analysis of the Oxidized Rim Material from the Prototype Anode After Testing

peaks for Cu indicated that the metal phase had a composition slightly more Cu-rich (70% Cu) than the starting material. Since no diffraction peaks from Ni metal were found in the x-ray pattern, some of the Ni in the metal phase probably was oxidized to NiO. It is also possible that the amount of Ni was small enough to be below the detection limits of the SEM analyzer and XRD.

Chemical and SEM analyses were performed at various areas within the anode rim. The chemical analyses were used to support the SEM analyses. In the oxide layer that formed on the inside of the anode cup, only chemical analyses were performed. The results from the chemical analyses indicated

that the overall composition had not changed drastically, although the x-ray analysis showed that the Cu metal had been oxidized to CuO.

In the cermet portion of the anode rim, both SEM and chemical analyses indicated that the material was slightly more rich in Ni, but this result was difficult to substantiate. Figure 4.16 shows that the material in this zone had undergone some structural reorganization, which resulted in an increased porosity. In these SEM photographs, the lightest-appearing materials contain Cu; the next lightest contain mostly Ni; and the darkest-appearing grains ,contain mostly Fe. Figure 4.17 shows a grain of material that appears to have partly reacted. It is uncertain if this particular grain was high in Fe or Ni at the start of the reaction. However, the general appearance of the grains shown in Figure 4.16 indicates restructuring.

At the interface between the cermet and the oxide formed on the outside of the anode rim, the SEM analyses indicate that the overall composition was the same as that found in the interior of the cermet. In the oxidized portion immediately adjacent to the cermet, the Cu content was reduced to about 7%. Presumably, the Cu was present in this zone as CuO based on the x-ray results.

At the surface of the anode rim, the analytical results become somewhat confusing. There are indications that both Cu and Ni were being removed from the anode. Also, elements from the electrolyte infiltrated the outer region of the oxidized zone and the porosity increased dramatically. Instead of phases being readily delineated by contrast, the phases seem to have about the same average atomic number and, hence, nearly the same grey tone. This result indicates that the phases were becoming homogeneous with respect to the Fe and Ni contents. An SEM photomicrograph of a typical portion of the surface is shown in Figure 4.18. An XRD pattern of the surface material (Figure 4.19) shows the presence of NaF, Na_3AlF_6, CaF_2, Al_2O_3 (both beta and alpha), and two copper aluminate phases ($CuAl_2O_4$ and $CuAlO_2$) in addition to the anode phases. These results indicate that the cermet was reacting with the vapors above the cryolite and that Cu(I) and Cu(II) were present. Copper and nickel were transported through the oxidized zone and probably volatilized as fluorides.

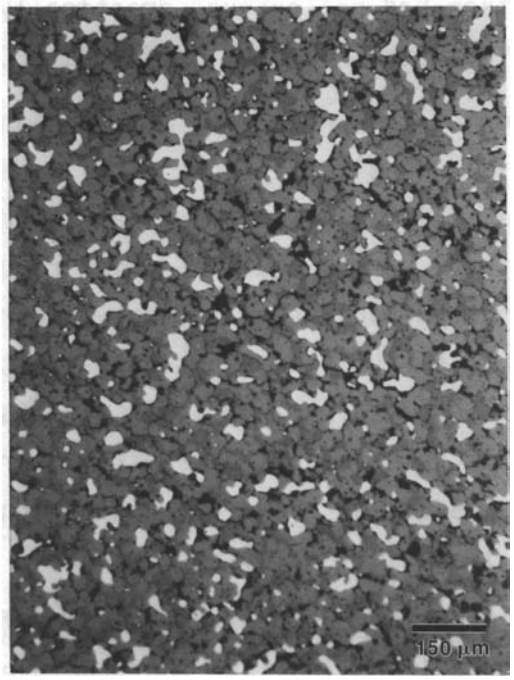

FIGURE 4.16. SEM Photomicrograph of the Cermet Portion of the Oxidized Rim of the Prototype Anode

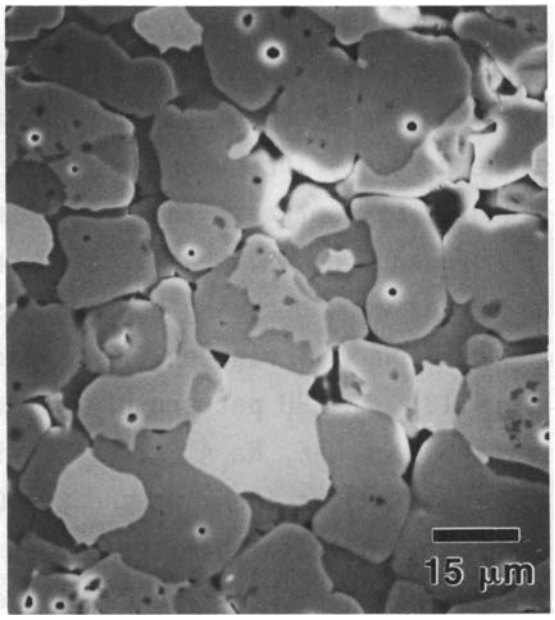

FIGURE 4.17. Photomicrograph at Larger Magnification of a Grain Shown in in Figure 4.16

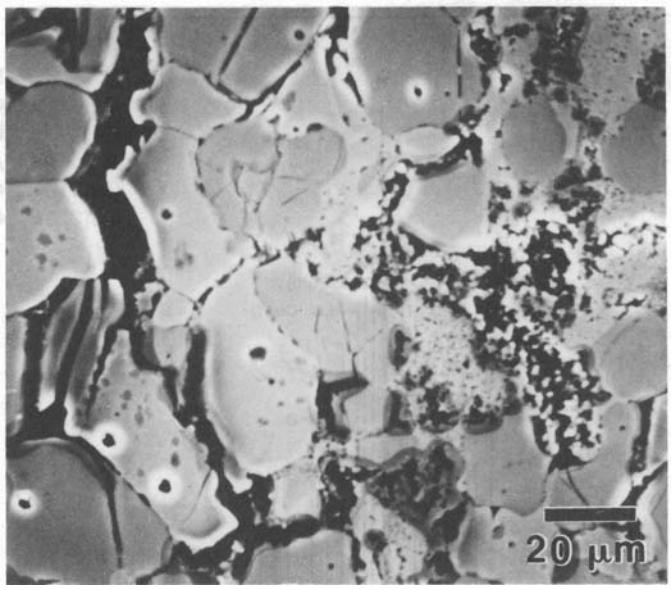

FIGURE 4.18. SEM Photomicrograph of the Immediate Surface of the Oxidized Rim Material on the Prototype Anode

4.2.2 Melt Line

A photomicrograph of the sample taken from the region of the anode at the electrolyte/air interface is shown in Figure 4.20. Here oxidation is not apparent, but there is a thin halo of copper-colored material near the surface (again, not seen in this photo). It is unlikely that any significant quantity of oxide material was lost when the crust was stripped, since the dimensions of the anode at this point were the same as before electrolysis.

More oxidation appeared to have occurred on the inside of the cup portion of the anode that was filled with Al_2O_3. Copper was depleted in this region and distinction (contrast) between Fe-rich and Ni-rich phases was absent, indicating that the Fe and Ni distributions were becoming more homogeneous. While the Ni concentrations usually exceeded the Fe concentrations in the cermet, the Fe concentration exceeded the Ni concentration in the oxidized area near the inside of the cup. Some Al, about 3.5 wt%, was also found in this area. The central part of this specimen appeared to be unchanged from the original cermet.

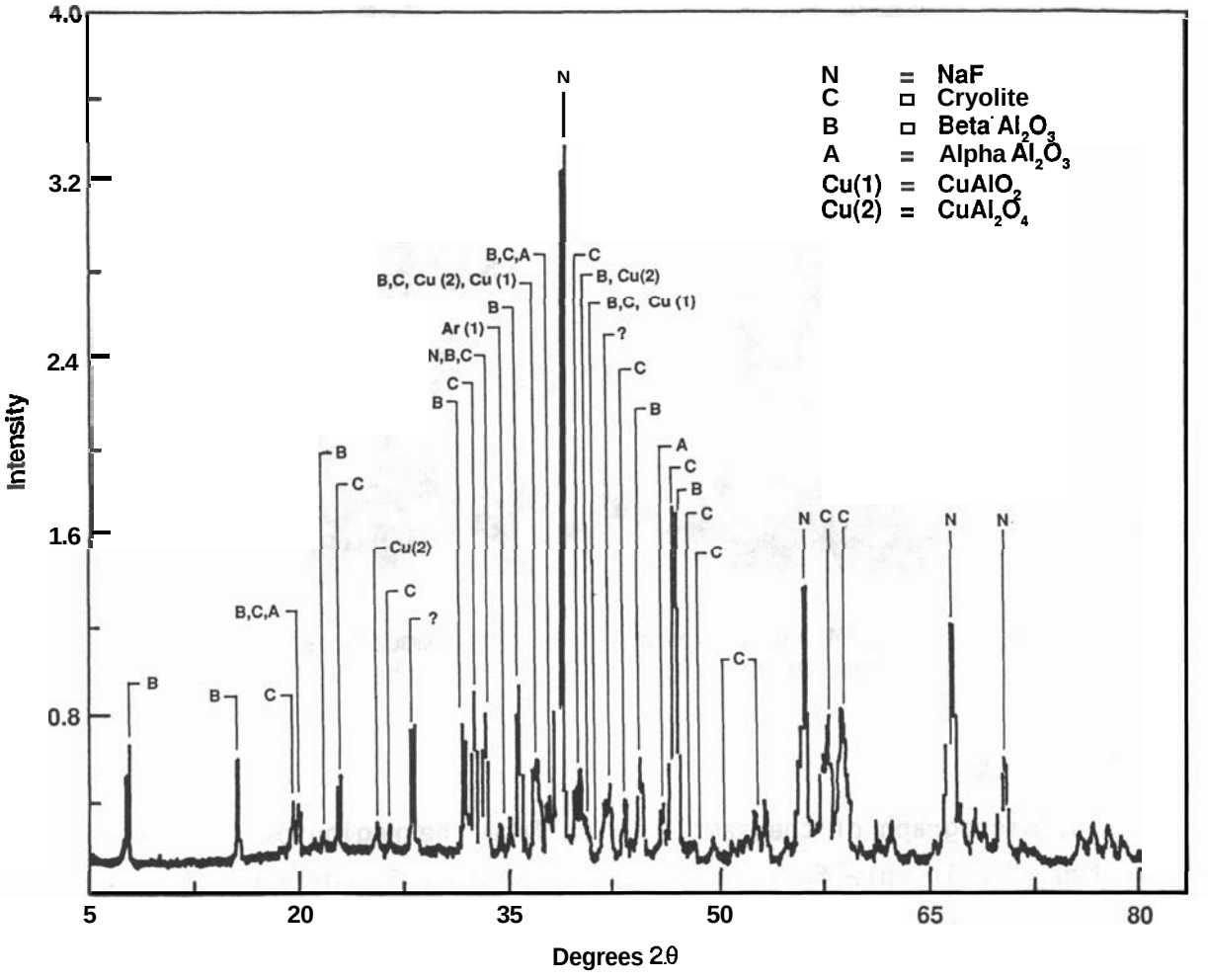

FIGURE 4.19. Results from the XRD Analysis of the Immediate Surface of the Oxidized Layer of the Prototype Anode Rim

4.2.3 Electrolysis Surfaces

Figure 4.21 is a photomicrograph of the specimen used to characterize the surfaces where electrolysis took place. The surface below the melt line is characterized by a dark area approximately 3 mm in thickness that tapers near the anode-electrolyte-air interface. Interior to the anode from this surface is a Cu-colored zone. Phase analyses using x-ray diffraction show that the surface rind contains NiO, spinel ($NiFe_2O_4$), and Cu_2O (Figure 4.22). From XRD analyses, the Cu-colored area in the cermet was found to contain a metallic phase that is nearly pure Cu (>95%). Although the SEM analyses show that Cu is depleted in the surface rind, an analysis obtained by dissolving a

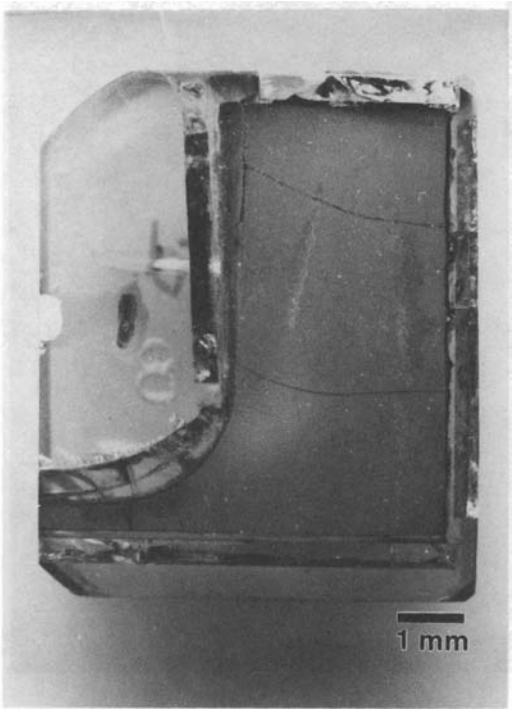

FIGURE 4.20. Photomicrograph of the Prototype Anode at the Melt Line

sample of the surface rind and quantifying the concentrations in the resulting solution indicates that the bulk composition did not change much from the original cermet. Depletions were noted for both Cu and Ni.

The appearance of a Cu-colored zone indicated that the Ni was selectively oxidized from the metallic phase to yield a phase richer in Cu. Consequently, a set of SEM energy dispersive x-ray analyses were performed in the SEM on the metallic phase starting at the surface rind-cermet interface and progressing interior to the anode at 1-mm intervals. The results from these analyses are shown in Figure 4.23. These results corroborate the x-ray analyses, which also indicate that the Cu-colored zone seen in the anode after the test was probably due to the selective oxidation of Ni from the alloy.

4.2.4 Electrical Connection

Figure 4.24 shows the area in which the electrical connection was made between the 25-mm Ni rod and the anode cermet. The connection area between

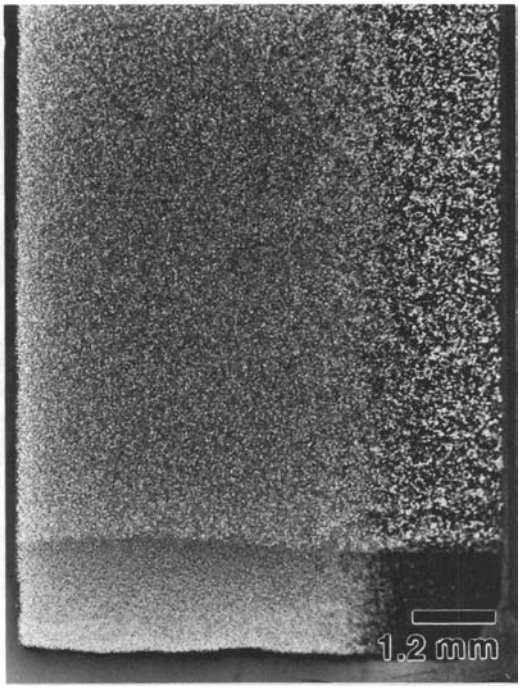

FIGURE 4.21. Photomicrograph of the Prototype Anode Electrolysis Surface

the sintered alloy and the cermet is detailed in Figure 4.25. The crack between the two materials most certainly occurred on cooling the anode and during the cutting and polishing operations. Diffusion of the Cu/Ni alloy into the cermet can also be seen in Figure 4.25. Figure 4.26 is an enlargement of the central portion of the sample shown in Figure 4.25 and more clearly shows the migration of the Cu/Ni alloy into the cermet. On the left side of the photomicrograph (Figure 4.26) the light areas are pure Cu/Ni alloy and the darker areas are the ferrite phase ($NiFe_2O_4$). On the right side of the photomicrograph, a typical cermet, three-phase system is observed. Apparently, as the Cu/Ni alloy migrates, the NiO phase is consumed.

A Cu-rich area was found where the Cu/Ni alloy was in contact with the Al_2O_3 fill material. This phase was pure Cu. Below this area of pure Cu was a two-phase region of pure Cu and NiO. These results support the earlier assumption that Ni was being selectively oxidized from the metal phase in the cermet to form pure Cu and NiO.

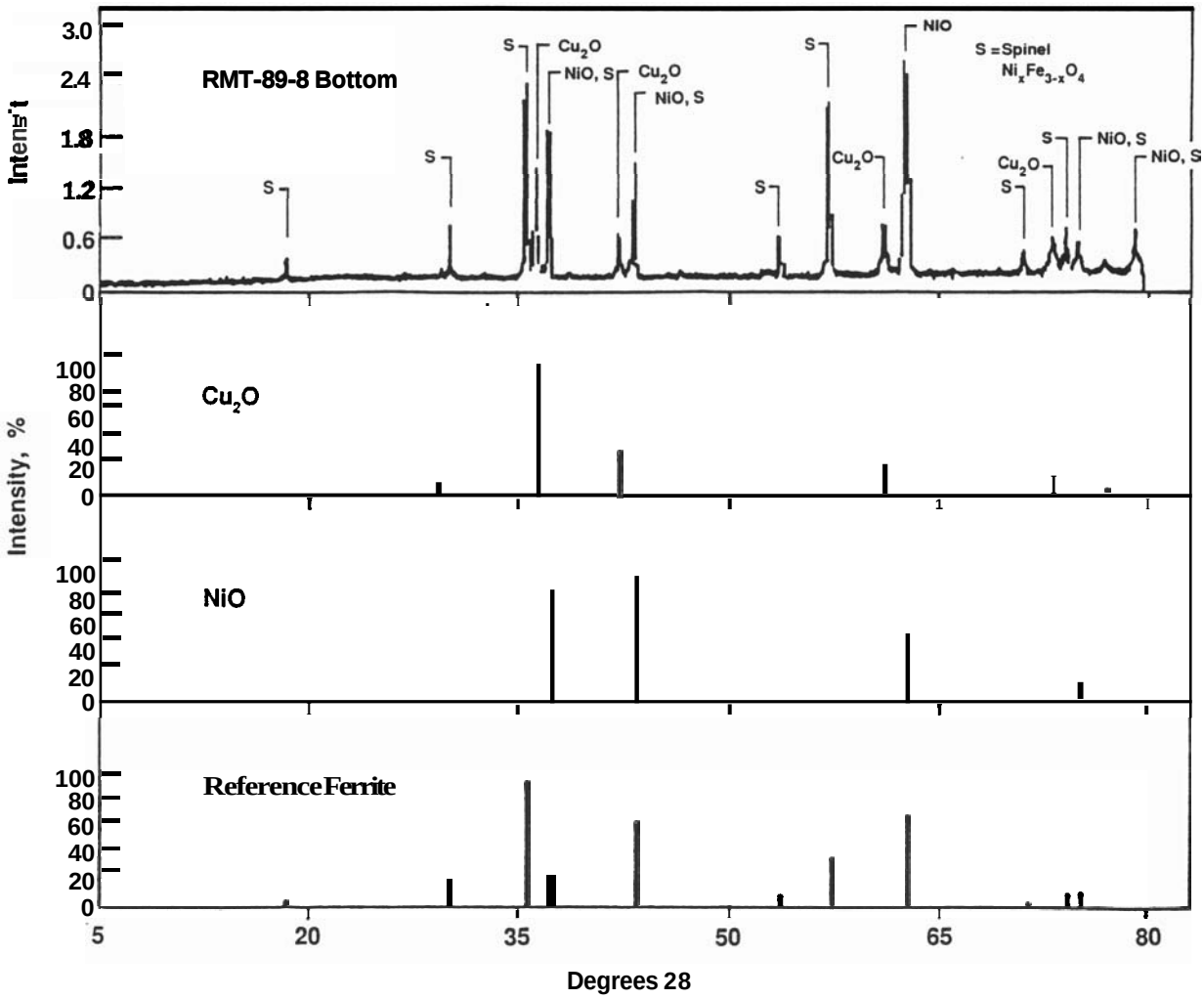

FIGURE 4.22. Results from the XRD Analysis of the Oxidized Material on the Electrolysis Surface of the Prototype Anode

4.3 SIGNAL MONITORING

4.3.1 Digital Signal Analysis

In his analysis, Dr. Nikias investigated the performance of advanced DSA methods based on both linear and nonlinear signal modeling techniques when they are applied to the analysis of aluminum smelting data, specifically cell current and voltage signals. The principal objective was to identify and measure the effect of signal quantification parameters that are sensitive to changes in the values of such electrochemical parameters as alumina

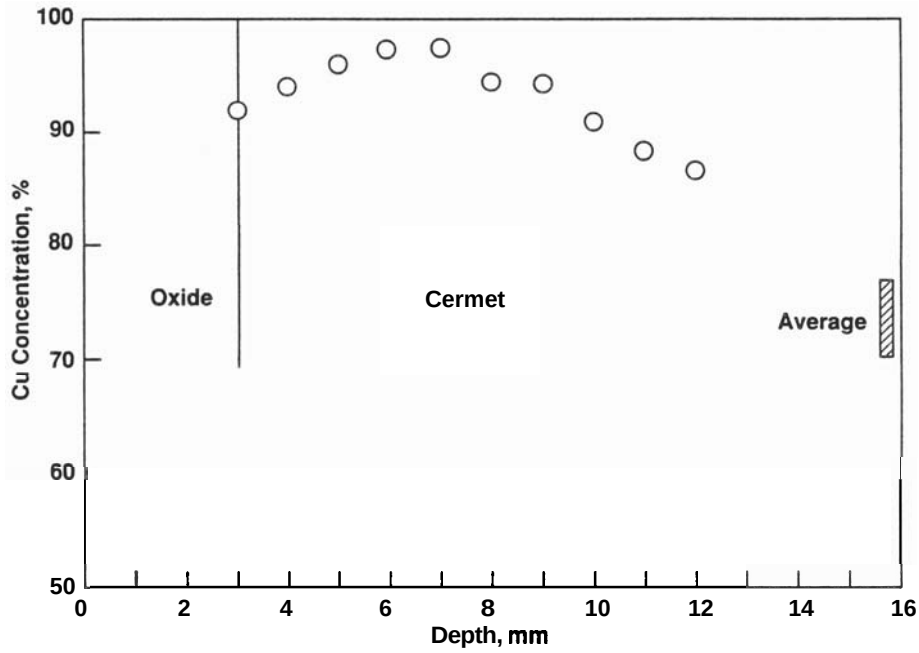

FIGURE 4.23. Results from Energy Dispersive X-Ray Analyses in the SEM of the Metallic Phase near the Electrolysis Surface. These analyses were performed at 1-mm intervals starting at the rind-cermet interface and proceeding toward the interior of the anode.

concentration, current density, bath ratio, and temperature. The quantification parameters may turn out to be useful as non-invasive process control methods capable of providing real-time information on cell conditions. This, in turn, will assist in maximizing the efficiency of commercial aluminum smelting operations.

Short-term experiments conducted with PNL bench-scale laboratory cells are being performed largely to establish whether correlations exist between the DSA-derived quantification parameters and cell operating conditions. Laboratory cells at PNL are being used because their operating conditions, specifically current density and bath composition, can be adjusted more easily and controlled more precisely than in large-scale cells.

The principal issue regarding correlations for data from bench-scale cells is whether they can be applied with confidence to large-scale cells. Consequently, the approach taken for the analysis of the prototype anode data

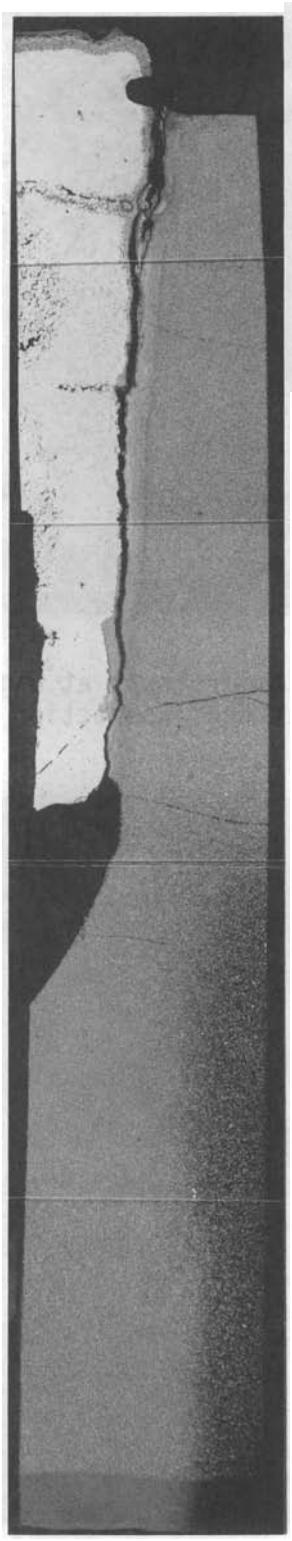

FIGURE 4.24. **Photomicrograph of the Electrical Connection Area of the Prototype Anode**

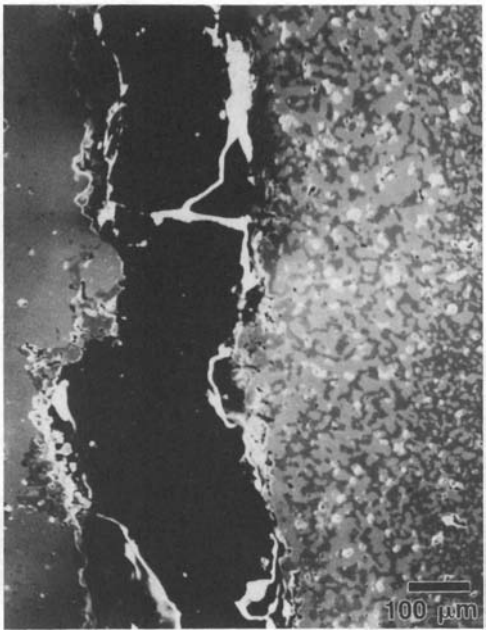

FIGURE 4.25. SEM Photomicrograph at Higher Magnification of the Electrical Connection Shown in Figure 4.24

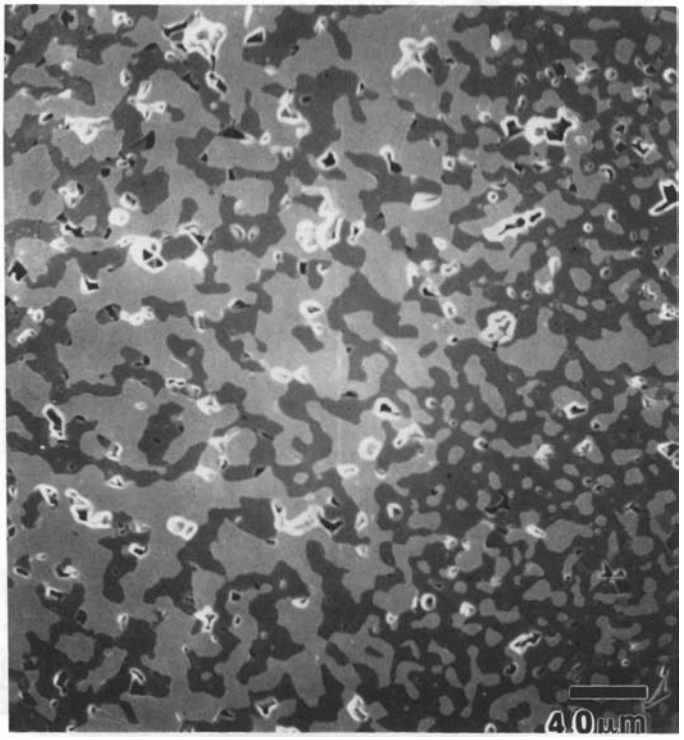

FIGURE 4.26. SEM Photomicrograph at Higher Magnification of the Area Shown in Figure 4.25

was to determine the quantification parameters for these data and then compare them to quantification parameters and their correlations with cell operating conditions for PNL laboratory data. Similarities in these quantification parameters is interpreted to suggest a correlation with general applicability to aluminum reduction cells using inert anodes with no significant effect caused by scale-up.

Four DSA techniques have been used to analyze current and voltage signals from bench-scale PNL laboratory cells: the Welch (Fast Fourier Transform-based) method, the Yule-Walker (YW) Autoregression method, the Magnitude-Squared Coherence (MSC) method, and nonlinear second-order Volterra modeling. Among the set of ad-hoc quantification parameters that have been identified from these methods, the two that show the best correlation with cell operating parameters appear to be R(o), the total power of the signals, and P(1)/R(o), a parameter related to the shape of the signals. Both of these quantification parameters obtained from low-passed (<25 Hz) voltage signals appear to show some correlation with working anode current density. The correlations were observed over a range of alumina concentrations.

The correlations observed for R(o) and P(1)/R(o) for low-passed.voltage signals were as follows:

- R(o) decreased slightly when the current density changed from 0.1 to 0.5 A/cm^2 and then increased with current density above 0.5 A/cm^2. The most dramatic increase occurred when the current density changed from 1.5 to 2.0 A/cm^2.
- P(1)/R(o) increased slightly when the current density changed from 0.1 to 0.5 A/cm^2 and then decreased when current density exceeded 0.5 A/cm^2.

The above correlations for bench-scale PNL laboratory data are shown in Figures 4.27 through 4.30.

Preliminary analyses of the prototype anode data as reported by Dr. Nikias indicated that most of the time signals for current and voltage for the prototype anode test contained several spikes or impulses that did not seem to correlate with cell operating conditions. The presence of the spikes caused severe changes in the values of the estimated quantification parameters.

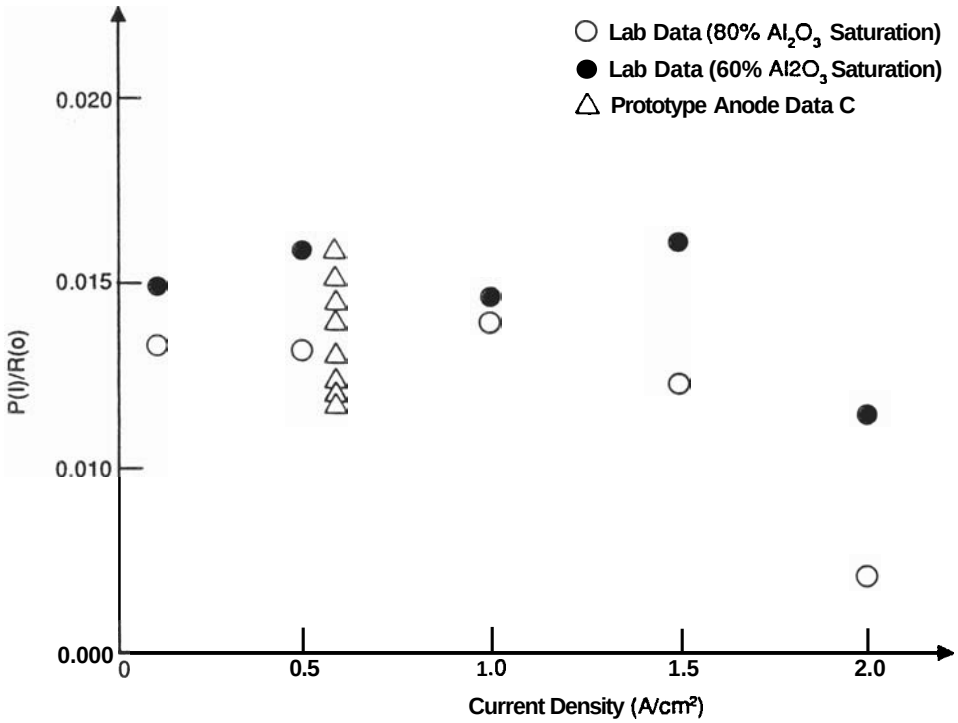

FIGURE 4.27. Parameter R(o): Comparison for Prototype Anode Data B Low-Passed Voltage Signals

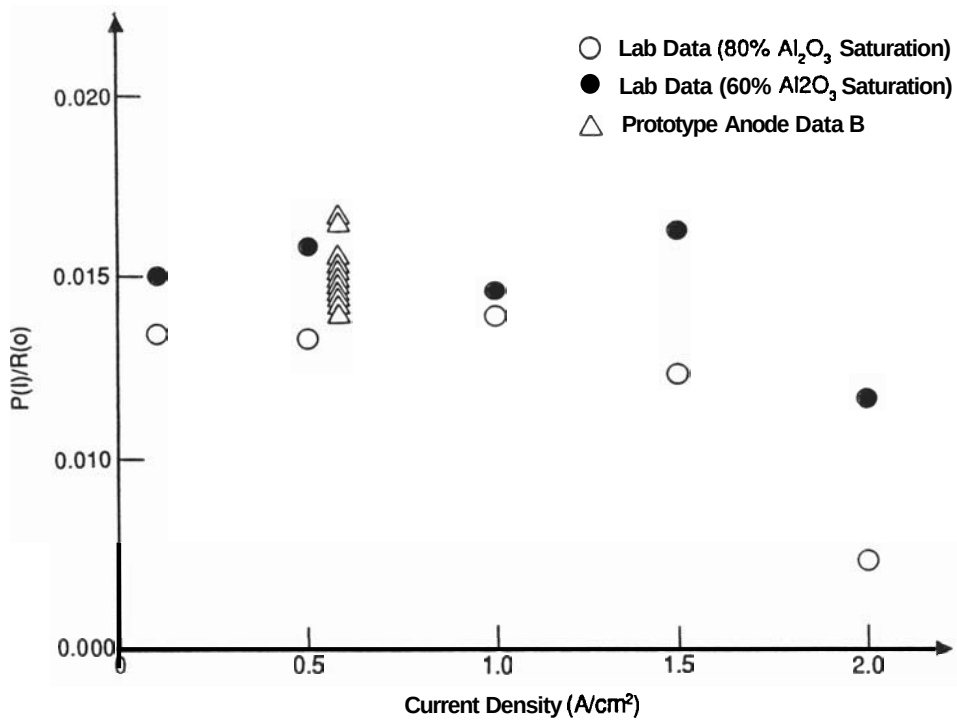

FIGURE 4.28. Parameter R(o): Comparison for Prototype Anode Data C Low-Passed Voltage Signals

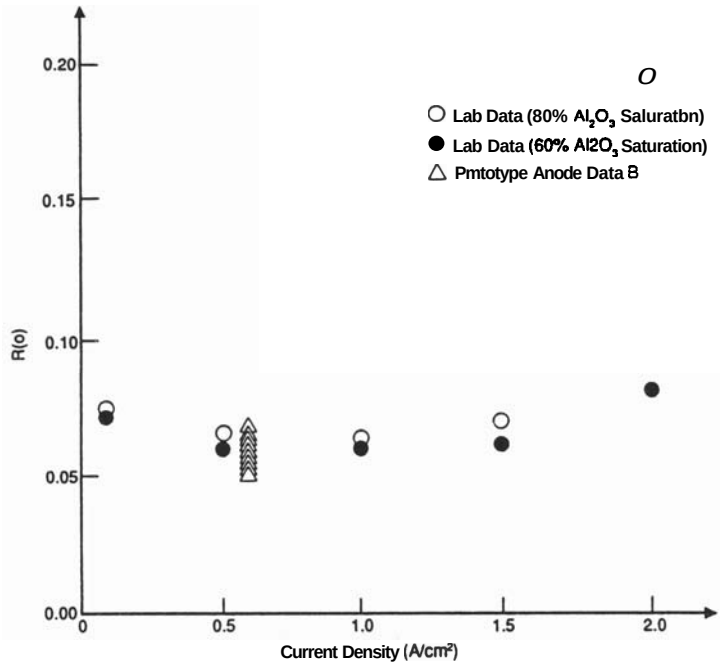

FIGURE 4.29. Parameter P(1)/R(o): Comparison for Prototype Anode Data B Low-Passed Voltage Signals

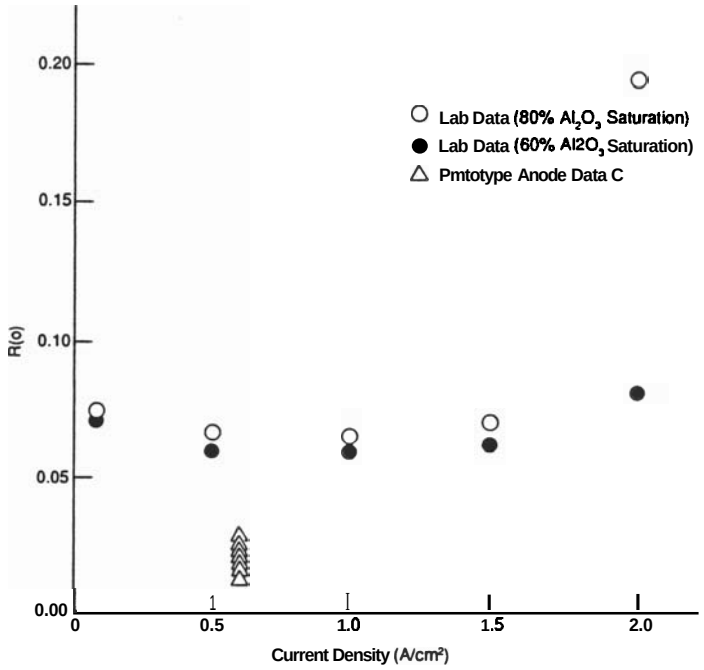

FIGURE 4.30. Parameter P(l)/R(o): Comparison for Prototype Anode Data C Low-Passed Voltage Signals

Reexamination of the prototype anode data after selecting data between the spikes for analysis, however, did suggest correlations that were consistent with those observed for PNL bench-scale laboratory data. Specifically, the following observations were made by Dr. Nikias:

- The signal parameter **P(1)/R(o)** for the prototype anode voltages B and C (refer to Section **3.2** for notation) takes approximately the same values as **P(1)/R(o)** of the PNL bench-scale laboratory voltage data. The "spread" that is observed in the values of **P(1)/R(o)** is perhaps due to changes in bath ratio and % Al_2O_3 during the data collection processes.
- The signal parameter **R(o)** for the prototype anode voltage B takes approximately the same values with **R(o)** of the PNL bench-scale laboratory voltage data. However, the **R(o)** of the prototype anode voltage C takes values that are approximately **30%** of those from the PNL bench-scale laboratory voltage data.

To illustrate the above consistencies between the prototype anode data and the PNL bench-scale laboratory data, the two are plotted together in Figures **4.27** through **4.30.** As indicated above, the quantification parameters for the prototype anode voltages B and C **[(P(1)/R(o)** only], which were obtained at a nominal current density of **0.6** A/cm^2, fall in a range consistent with a similar current density for the PNL bench-scale laboratory data. These results suggest that the observed correlations are general and not strongly dependent on scale-up considerations.

The prototype anode signals B and C are both cell voltages and differ only in where the anode tap was made. For B, the anode tap was at the anode stem, while for C, the tap was on the inner surface of the working anode. It is reasonable that these voltage signals showed some correlation with the current density since electrode processes that influence the extent of voltage noise may vary over the range of current densities studied. It is not clear, however, why C in the case of **R(o)** showed poor correlation, although it may have to do with the integrity of the inner anode connection. Lack of correlation of A is not surprising since the cell was under current control and consequently the contribution of process-derived noise to this signal was less. Lack of correlation of D may be explained by the less-than-adequate performance of the reference anode.

4.3.2 Analog Data Analysis

Analog data for the various voltages and currents measured with strip chart recorders (see Section 3.2) were generally stable except for periods when parameters were deliberately adjusted. For example, current versus voltage sweeps (reported earlier in this report) were occasionally performed during cell operation for diagnostic purposes. All of these data indicated no serious instabilities or deviations from what would be considered correct cell operation. It is not clear, at this time, why there was no indication in the analog data of the corrosion processes the inert anode clearly underwent. It is possible the larger size of the anode (compared with laboratory cells) gave a different sensitivity to these processes, but adequate size-effects data are lacking for definitive conclusions.

4.3.3 Reference Anode

Four reference anodes were used in sequence during the course of the prototype anode test. Two of the reference anodes were recovered. Two fell into the reduction cell as a result of catastrophic corrosion of their connector rods. Post-test examination of the recovered reference anodes showed that both had corroded severely during their time in the cell. Figure 4.31 shows the extent of corrosion in one case.

The corrosion of the reference anode occurred even though a small anodic current was passed through it. It was assumed that such a current should foster the formation of a protective layer and thus minimize corrosion of inert anodes.

Due to constraints involving the larger reduction cell, the mode of operation chosen for the reference anode was constant voltage control. Previous tests had involved cyclically shunting the reference anode to the working anode to maintain the small anodic current. Under voltage control, the current required to maintain a protective layer on the reference anode was assumed to be determined by the reference anode surface area exposed to the molten bath and by the alumina content of the bath as well as the control voltage. The control voltage was established by summing the theoretical open circuit cell voltage, the IR drop to the location of the reference anode (determined by the electrolyte resistance and the operating current), and the

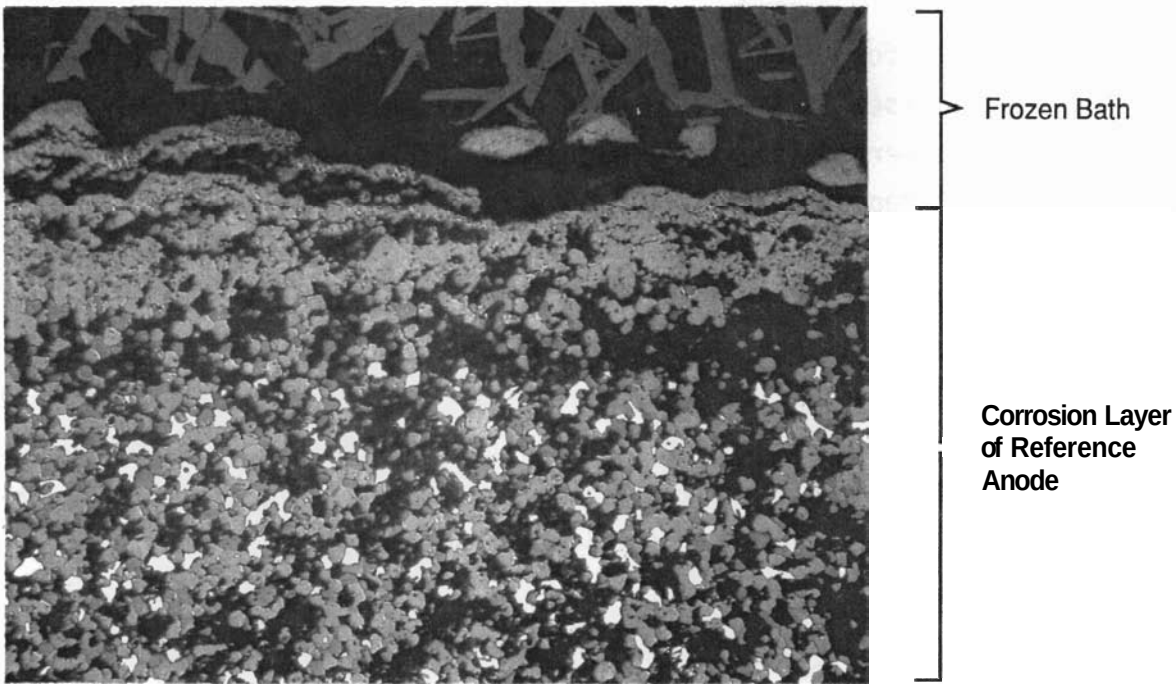

FIGURE 4.31. Corrosion of Reference Anode

cathode overvoltage at the operating current. The current required by the reference anode was recorded and assumed to be determined largely by the protective layer resistance and hence the alumina concentration. This assumes that the protective layer is dynamic in nature and has a resistance that is related to the alumina content of the bath, inversely proportional to the reference anode surface area exposed to the molten bath, and functionally related to the control voltage.

It was observed that the reference anode current was only slightly affected by the magnitude of the process current, although the control voltage used was considered to be less than its minimum value. The IR drop in the electrolyte subsequently could not be measured as a result of the dissolution and loss of integrity of the alumina cell liner. The reference anode current was generally noisy with a stable long-term trace, suggesting stable alumina content. An attempt to verify the response of the reference anode to variable alumina content was made during the termination of the experiment by stopping the addition of alumina. The results were

inconclusive, however, since the alumina liner continued to dissolve and maintain an almost constant alumina content in the bath. In addition, the cell furnace failed before the alumina content changed significantly.

Other problems encountered during the test included a persistent variation of the surface area of the reference anode exposed to the molten bath, the condensation of electrically conducting bath vapors on all exposed surfaces, and the formation of a "bridge" of frozen bath above the surface of the molten bath that caused electrical shunting during the test.

These results suggest that, despite the amount of research expended in FY 1989 on the development of the reference anode, serious issues regarding the operation of the electrode and of its durability remain. The most important of these issues are summarized below:

- The viability of the reference anode in the prototype anode test was inconclusive at best. No significant indication was given by the reference anode that the working anode was experiencing severe corrosion.
- The effects of the working anode size on the magnitude and quantity of the protective layer-breakdown signals have not been fully determined.
- Since the reference anode must be operated with a small current flowing through it, a reliable circuit has to be designed to give this current and also to keep the reference anode potential constant. It is not clear whether this approach is even possible in an operating cell. Attempts to do this in the prototype anode test gave questionable results.
- The reference anode design has some serious mechanical problems incurred by--among other factors--the difficulty in joining the connector rod to a long, narrow cermet electrode.

5.0 REFERENCES

Baker, F. W. 1983. Inert Anodes for Aluminum Smelting, Final Technical Report for the Peri'od 1981 October 01 - 1982 September 30. DOE-CS-40158, Aluminum Company of America, Alcoa Center, Pennsylvania.

Burgman, J. W., J. A. Leistra, and P. J. Sides. 1986. "A Reference Electrode for Hall Cell Experiments. In Light Metals 1986, The Minerals, Metals, and Materials Society, Warrendale, Pennsylvania.

Goodes, C. G., and S. H. Algie. 1989. "The Partitioning of Trace Impurities Between Aluminum, Cryolite and Air - A Laboratory Study." In Light Metals 1989, Paul G. Campbell, editor, The Minerals, Metals, and Materials Society, Warrendale, Pennsylvania.

Hart, P. E., B. B. Brondon, N. C. Davis, O. H. Koski, S. C. Marschman, K. H. Pool, C. H. Schilling, C. F. Windisch, and B. J. Wrona. 1987. Inert Anode/Cathode Program Fiscal Year 1986 Annual Report, PNL-6247, Pacific Northwest Laboratory, Richland, Washington.

Marschman, S. C. 1989. Laboratory-Scale Testing of Non-Consumable Anode Materials. PNL-6805, Pacific Northwest Laboratory, Richland, Washington.

Strachan, D. M., O. H. Koski, S. C. Marschman, C. H. Schilling, and C. F. Windisch. 1988. Inert Electrodes Program Fiscal Year 1987 Annual Report. PNL-6746, Pacific Northwest Laboratory, Richland, Washington.

Strachan, D. M., S. C. Marschman, N. C. Davis, J. R. Friley, and C. H. Schilling. 1989. Inert Electrodes Program Fiscal Year 1988 Annual Report. PNL-7106, Pacific Northwest Laboratory, Richland, Washington.

Weyand, J. D., D. H. DeYoung, S. D. Ray, G. P. Tarcy, and F. W. Baker. 1986. Inert Anodes for Aluminum Smelting. Final Technical Report for the Period 1980 September 29 - 1985 September 30. DOE-CS-40158-20, Aluminum Company of America, Alcoa Center, Pennsylvania.

APPENDIX

MASS BALANCES FOR THE CELL

TABLE A.1.1. Mass Balance Sheet and Results from Analyses of Electrolyte Samples

			Bath Input and Output								
Date	Tim	Event	Input (g)	Output (g)	Sample ID	Ratio	%AL203	CaF2	Cu	Fe	Ni
3-17-89	3.00	add bath	11000	0.00							
3-19-89	3.15	sample taken	0	35.58	2476-12-1	1.27	9.82	6.12	0.0028	0.13	0.027
	4.45	sample taken	0	14.76	2476-13-1	1.27					
	5.30	add NaF	168	0							
	6.05	sample taken	0	12.61	2476-13-2	1.35					
	6.25	sample taken	0	42.70	2476-14-1	1.27	7.14	5.49	0.0005	0.058	0.0028
	10.40	sample taken	0	38.24	2476-17-1	1.22	7.03	5.46	0.0013	0.037	0.0039
	11.31	add NaF	168	0							
	15.55	ample taken	0	33.09	2476-19-1	0.99	8.3	4.88	0.0001	0.023	0.0016
	17.00	add NaF	105	0							
	17.20	add NaF	105	0							
	17.40	add NaF	105	0							
	18.00	add NaF	105	0							
	18.20	add NaF	105	0							
	18.40	add NaF	105	0							
	20.15	sample taken	0	21.00	2476-20-1	1.18	6.07	4.94	0.007	0.024	0.0034
	23.15	ample taken	0	24.72	2476-21-1	1.03	3.91	5.07	0	0	0
3-20-89	1.30	add NaF	105	0							
	2.15	add NaF	105	0							
	2.50	add NaF	105	0							
	3.22	sample taken	0	47.11	2476-24-1	1.06	2.86	4.38	0.004	0.017	0.0009
	5.18	add Al203	125	0							
	6.56	add Al203	109.4	0							
	8.00	sample taken	0	39.71	2476-25-1	0.94	3.14	4.4	0.005	0.017	0.0009
	8.05	add bath	2000	0							
	8.30	add Al203	20	0							
	9.10	add NaF	1%	0							
	9.16	add Pilot bath	500	0							
	9.35	add Al203	100	0							
	10.04	add bath	245	0							
	10.28	add bath	255	0							
	10.28	add Al203	100	0							
	10.40	add NaF	236	0							
	11.05	add NaF	211	0							
	11.05	add Al203	100	0							
	11.37	add NaF	220	0							
	14.45	sample taken	0	69.98	2476-27-1	1.50	7.18	4.24	0.0008	0.015	0.0008
	17.14	sample taken	0	64.69	2476-28-1	1.49	7.11	4.07	0.0069	0.043	0.0098
	17.58	add Al203	11	0							
	18.10	add Al203	11	0							
	18.25	add Al203	11	0							
	19.00	add Al203	11	0							
	19.15	add A1203	11	0							
	19.30	add Al203	11	0							
	19.45	add Al203	11	0							
	20.00	add Al203	11	0							
	20.10	sample taken	0	58.40	2476-29-1	1.45	8 .	4.2	0.0063	0.057	0.015
	21.00	add bath	150	0							
	21.40	add Al203	15	0							
	22.25	add bath	310	0							
	22.35	sample taken	0	30.00	2476-31-1	1.45	8.03	4.62	0.003	0.033	0.0086
	22.50	add bath	300	0							
	23.15	add bath	300	0							
	23.53	add bath	300.25	0							
3-21-89	0.28	add bath	300	0							
	0.38	sample taken	0	44.08	2476-32-1	1.43	7.99	4.71	0.134	0.17	0.355
	1.07	add bath	150	0							
	1.07	add Al203	50	0							
	1.55	add bath	150	0							
	1.55	add Al203	50	0							
	2.30	sample taken	0	43.14	2476-32-2	1.42	8.53	4.43	0.049	0.093	0.128
	2.55	add bath	150	0							
	3.25	add Al203	10	0							
	3.41	add Al203	10	0							
	4.05	add Al203	10	0							
	4.23	sample taken	0	33.11	2476-33-1	1.40	7.95	3.97	0.0054	0.045	0.012
	4.26	add A1203	15	0							
	5.12	add bath	200	0							
	5.42	add Al203	10	0							
	5.53	add Al203	10	0							
	5.57	add A1203	20	0							
	6.05	add Al203	20	0							

TABLE A.1.1. (contd)

	6.15	add bath	150	0							
	6.15	add Al203	20	0							
	6.36	sample taken	0	43.27	2476-34-2	1.40	8.6	3.9	0.011	0.054	0.024
	6.40	add Al203	20	0							
	7.00	add Al203	20	0							
	7.20	add Al203	20	0							
	8.20	sample taken	0	50.70	2476-35-1	1.36	7.73	4.6	0.035	0.116	0.064
	8.45	add bath	250	0							
	8.45	add Al203	15	0							
	9.08	add bath	250	0							
	9.08	add Al203	15	0							
	10.00	add bath	250	0							
	10.00	add Al203	15	0							
	10.36	add bath	300	0							
	10.36	add Al203	15	0							
	10.38	sample taken	0	40.45	2476-36-2	1.36	7	4.71	0.0053	0.036	0.013
	11.09	add bath	250	0							
	11.09	add Al203	15	0							
	11.30	add bath	250	0							
	11.30	add Al203	15	0							
	12.03	add bath	250	0							
	12.03	add Al203	15	0							
	12.50	add Al203	15	0							
	13.20	add Al203	15	0							
	13.55	add Al203	15	0							
	14.30	add Al203	15	0							
	15.03	sample taken	0	37.90	2476-38-1	1.34	7.7	3.02	0.015	0.074	0.036
	15.07	add Al203	15	0							
	15.40	add bath	250	0							
	15.40	add Al203	15	0							
	16.15	add Al203	15	0							
	16.45	add bath	250	0							
	16.45	add Al203	15	0							
	17.07	sample taken	0	36.47	2476-39-1	1.34	7.91	4.74	0.011	0.032	0.024
	17.20	add Al203	15	0							
	17.45	add bath	250	0							
	17.45	add Al203	15	0							
	18.15	add Al203	15	0							
	18.45	add Al203	15	0							
	19.15	add A1203	15	0							
	19.55	sample takm	0	37.32	2476-40-1	1.32	7.59	4.95	0.0027	0.018	0.013
	21.00	add Al203	15	0							
	21.05	add bath	250	0							
	21.45	add Al203	15	0							
	22.25	add Al203	15	0							
	22.45	sample takm	0	33.14	2476-43-1	1.3	6.45	4.95	0.0002	0.024	0.0077
	23.00	add bath	250	0							
	23.05	add Al203	15	0							
	23.30	add Al203	15	0							
3-22-69	0.11	add Al203	15	0							
	0.45	add Al203	15	0							
	1.00	sample taken	0	32.09	2476-44-1	1.33	7.74	4.89	0.024	0.06	0.057
	1.03	add Al203	15	0							
	1.03	add bath	150	0							
	1.22	add Al203	15	0							
	1.45	add Al203	15	0							
	2.06	add bath	150	0							
	2.06	add Al203	15	0							
	2.35	add Al203	15	0							
	3.21	add Al203	15	0							
	3.47	add Al203	15	0							
	4.07	sample taken	0	26.82	2476-45-2	1.32	7.48	4.78	0.003	0.016	0.006
	4.30	add Al203	15	0							
	5.06	add Al203	15	0							
	5.06	add bath	150	0							
	5.55	add Al203	15	0							
	6.22	add A1203	15	0							
	6.50	sample taken	0	36.31	2476-46-2	1.26	7.64	4.55	0.0004	0.018	0.0009
	6.52	add bath	250	0							
	7.22	add Al203	15	0							
	9.44	add Al203	15	0							
	10.50	add Al203	15	0							
	11.05	add bath	250	0							
	11.29	sample taken	0	36.52	2476-48-1	1.28	7.53	4.76	0.004	0.018	0.0071
	11.39	add Al203	15	0							
	12.25	add Al203	15	0							

TABLE A.1.1. (contd)

	13.02	add A1203	15	0							
	13.30	add A1203	15	0							
	14.03	add Al203	15	0							
	14.35	add Al203	15	0							
	15.50	add A1203	15	0							
	15.50	add NaF	63	0							
	15.50	add bath	250	0							
	16.05	sample taken	0	30.17	2476-50-2	1.29	8.13	5.06	0.015	0.026	0.028
	16.20	add Al203	20	0							
	16.35	add A1203	20	0							
	16.40	add Al203	20	0							
	16.50	add Al203	20	0							
	16.55	add Al203	15	0							
	17.00	add bath	250	0							
	17.25	add A1203	20	0							
	17.50	add bath	250	0							
	17.50	add NaF	63	0							
	17.50	add A1203	15	0							
	18.31	add Al203	20	0							
	18.59	add Al203	20	0							
	19.18	sample taken	0	43.77	2476-52-1	1.27	7.55	4.96	0.0055	0.023	0.0095
	19.20	add Al203	20	0							
	19.40	add Al203	25	0							
	19.40	add b t h	250	0							
	19.55	add Al203	20	0							
	20.30	add A1203	25	0							
	21.05	add Al203	25	0							
	22.23	add A1203	30	0							
	22.30	sample tekm	0	37.02	2476-53-1	1.26	8.09	5.08	0.0078	0.026	0.014
	22.43	add bath	250	0							
	23.07	add Al203	30	0							
	25.40	add A1203	30	0							
3-23-89	0.00	add bath	250	0							
	0.08	add A1203	30	0							
	0.38	add NaF	105	0							
	1.10	add A1203	30	0							
	1.40	sample taken	0	34.21	2476-55-1	1.23	8.02	5.17	0.015	0.029	0.024
	1.43	add abth	250	0							
	2.17	add A1203	30	0							
	3.15	add Al203	30	0							
	4.08	add A1203	30	0							
	4.37	sample tekm	0	26.88	2476-56-2	1.23	8	5.18			
	4.38	add bath	250	0							
	5.50	add NaF	105	0							
	5.57	add A1203	30	0							
	6.55	add Al203	30	0							
	7.00	add bath	250	0							
	7.54	add bath	250	0							
	8.24	sample tekm	0	41.52	2476-58-1	1.26	7.77	5.07	0.14	0.17	0.21
	8.42	add bath	250	0							
	9.38	add bath	250	0							
	9.38	add A1203	15	0							
	9.38	add NaF	148	0							
	10.27	sample tekm	0	20.50	2476-59-1	1.26	9.43	4.85	0.17	0.17	0.28
	11.18	add Al203	15	0							
	11.37	add A1203	15	0							
	11.45	add b t h	250	0							
	11.45	add Al203	15	0							
	12.18	add bath	250	0							
	12.18	add Al203	15	0							
	13.14	add Al203	15	0							
	14.23	add NaF	100	0							
	14.23	add Al203	15	0							
	14.50	sample tekm	0	20.00	2476-61-1	1.26	9.11	4.96	0.0088	0.095	0.0186
	15.29	add Al203	20	0							
	16.10	add A1203	20	0							
	16.35	add Al203	20	0							
	17.10	add A1203	25	0							
	18.10	add A1203	30	0							
	18.10	add NaF	100	0							
	19.15	sample taken	0	40.16	2476-62-1	1.32	8.46	4.73	0.05	0.1	0.077
	19.25	add Al203	30	0							
	20.00	add Al203	30	0							
	20.00	add bath	250	0							
	21.00	add Al203	30	0							
	21.00	add bath	250	0							

TABLE A.1.1. (contd)

	22.15	add A1203	30	0							
	22.45	add A1203	30	0							
	23.05	add Al203	30	0							
	23.05	add bath	250	0							
3-24-89	0.05	sample taken	0	39.78	2476-64-1	1.33	8.35	4.84	0.01	0.049	0.019
	0.10	add A1203	30	0							
	0.50	add Al203	30	0							
	0.52	add bmth	200	0							
	1.35	add Al203	30	0							
	2.30	add Al203	30	0							
	2.30	add bmth	200	0							
	3.00	add A1203	30	0							
	3.50	add A1203	30	0							
	5.00	add Al203	30	0							
	5.00	add bath	250	0							
	6.00	sample taken	0	31.40	2476-66-1	1.31	8.09	4.96	0.014	0.055	0.023
	6.01	add A1203	30	0							
	6.40	add A1203	30	0							
	7.15	add bath	250	0							
	7.25	add Al203	30	0							
	7.58	add Al203	15	0							
	8.38	add bath	250	0							
	8.38	add Al203	15	0							
	10.15	sample taken	0	37.17	2476-67-1	1 . 1	8.68	4.83	0.0066	0.032	0.012
	10.30	add Al203	15	0							
	11.15	add Al203	15	0							
	11.15	add bath	100	0							
	11.15	add NaF	100	0							
	13.18	add Al203	15	0							
	13.40	sample taken	0	24.58	2476-68-1		7.93	.			
	13.50	add A1203	15	0							
	14.M	add A1203	15	0							
	15.18	add Al203	15	0							
	16.15	add A1203	15	0							
	16.25	sample taken	0	15.99	2476-68-2		7.97	4.73	0.0142	0.0288	0.0081
	17.20	add Al203	15	0							
	18.50	sample taken	0	29.19	2476-70-1	1.29	8.75	4.71	0.0078	0.034	0.016
	18.56	add bath	250	0							
	19.50	sample taken	0	18.41	2476-70-3		7.6	4.95	0.0028	0.016	0.0057
	19.59	add bath	250	0							
	20.45	sample taken	0	34.70	2476-71-1		7.91	4.86	0.0027	0.015	0.0061
	21.45	sample taken	0	20.37	2476-71-2	1.26	7.51	4.95	0.016	0.038	0.041
	22.14	add bath	300	0							
	22.45	sample taken	0	21.11	2476-71-3		7.83	5.011	0.007	0.025	0.014
	23.31	add bath	300	0							
	23.45	sample taken	0	32.48	2476-71-4	1.26	8.93	4.97	0.0041	0.019	0.0082
3-25-89	0.41	sample taken	0	20.00	2476-72-1		7.92	4.97	0.0035	0.02	0.0074
	0.45	add NaF	100	0							
	2.39	add bmth	300	0							
	3.10	sample taken	0	22.81	2476-72-2	1.31	7.52	5.06	0.014	0.042	0.029
	4.20	add bmth									
	5.55	sample taka	0	24.60	2476-73-1	1.29	8.37	4.94	0.0056	0.032	0.0099
	6.00	add bath	300	0							
	8.12	sample taken	0	19.40	2476-73-2		8.01	4.86	0.0035	0.018	0.007
	8.43	sample taken	0	20.00	2476-74-1		8 1	4.94	0.0043	0.024	0.0076
	9.16	sample taken	0	13.05	2476-74-2		8.18	4.95	0.0026	0.014	0.004

1820.67	Sample Amount
7268.00	Bulk Amount
2421.00	Amount on Anode
1181.00	Amount on Crucible Liner
1542.00	Loose Pieces
14232.67	Total

TABLE A.1.2. Results from Duplicate Analyses of Selected Electrolyte Samples

Date	Time	Decimal Day	Sample Output (g)	Sample ID	Ratio	%AL203	CaF2	Cu	Fe	Ni	Si
4-19-89	3.15	0.000	35.58	2476-12-1	1.27	9.82	6.12	0.0028	0.13	0.027	
	4.45	0.054	14.76	2476-13-1	1.27						
	6.05	0.121	12.61	2476-13-2	1.35						
	6.25	0.129	42.70	2476-14-1	1.27	7.14	5.49	0.0005	0.058	0.0028	0.012
	10.40	0.302	38.24	2476-17-1	1.22	7.03	5.46	0.0013	0.037	0.0039	
	15.55	0.517	33.09	2476-19-1	0.99	8.3	4.88	0.0001	0.023	0.0016	
	20.15	0.709	21.00	2476-20-1	1.18	6.07	4.94	0.007	0.024	0.0034	
	23.15	0.834	26.R	2476-21-1	1.03	3.91	5.07	0	0	0	
4-20-89	3.22	1.003	47.11	2476-24-1	1.06	2.86	4.38	0.004	0.017	0.0009	0.01
	8.00	1.202	39.71	2476-25-1	0.94	3.14	4.4	0.005	0.017	0.0009	
	14.45	1.471	69.98	2476-27-1	1.50	7.18	4.24	0.0008	0.015	0.0008	
	17.14	1.583	64.69	2476-28-1	1.49	7.11	4.07	0.0069	0.043	0.0098	
	20.10	1.707	58.40	2476-29-1	1.45	8.86	4.2	0.0063	0.057	0.015	
	22.35	1.800	30.00	2476-31-1	1.45	8.03	4.62	0.003	0.033	0.0086	0.012
4-21-89	0.38	1.885	44.08	2476-32-1	1.43	7.99	4.71	0.134	0.17	0.355	
	2.30	1.965	43.14	2476-32-2	1.42	8.53	4.43	0.049	0.093	0.128	0.03
	4.23	2.045	33.11	2476-33-1	1.40	7.95	3.97	0.0054	0.045	0.012	
	6.36	2.134	43.27	2476-34-2	1.40	8.6	3.9	0.011	0.054	0.024	
	8.20	2.211	50.70	2476-35-1	1.36	7.73	4.6	0.035	0.116	0.064	
	10.38	2.302	40.45	2476-36-2	1.36	7	4.71	0.0053	0.036	0.013	
	15.03	2.495	37.90	2476-38-1	1.34	7.7	3.02	0.015	0.074	0.036	
	17.07	2.580	36.47	2476-39-1	1.34	7.91	4.74	0.011	0.032	0.024	
	19.55	2.684	37.32	2476-40-1	1.32	7.59	4.95	0.0027	0.018	0.013	
	22.45	2.804	33.14	2476-43-1	1.3	6.45	4.95	0.0002	0.024	0.0077	
4-22-89	1.00	2.911	32.09	2476-44-1	1.33	7.74	4	0.024	0.06	0.057	
	4.07	3.039	26.82	2476-45-2	1.32	7.48	4.78	0.003	0.016	0.006	
	6.50	3.140	36.31	2476-46-2	1.26	7.64	4.55	0.0004	0.018	0.0009	
	11.29	3.339	36.52	2476-48-1	1.28	7.53	4.76	0.004	0.018	0.0071	0.007
	16.05	3.538	30.17	2476-50-2	1.29	8.13	5.06	0.015	0.026	0.028	
	19.18	3.668	43.77	2476-52-1	1.27	7.55	4.96	0.0055	0.023	0.0095	
	22.30	3.798	37.02	2476-53-1	1.26	8.09	5.M	0.0078	0.026	0.014	
4-23-89	1.40	3.927	34.21	2476-55-1	1.23	8.02	5.17	0.015	0.029	0.024	0.009
	4.37	4.051	26.88	2476-56-2	1.23	8	5.18				
	8.24	4.212	41.52	2476-58-1	1.26	7 .	5.07	0.14	0.17	0.21	0.02
	10.27	4.297	20.50	2476-59-1	1.26	9.43	4.85	0.17	0.17	0.28	
	14.50	4.473	20.00	2476-61-1	1.26	9.11	4.W	0.0088	0.095	0.0186	
	19.15	4.667	40.16	2476-62-1	1.32	8.46	4.73	0.05	0.1	0.077	0.016
4-24-89	0.05	4.871	39.78	2476-64-1	1.33	8.35	4.84	0.01	0.049	0.019	
	6.00	5.119	31.40	2476-66-1	1.31	8.09	4.96	0.014	0.055	0.023	
	10.15	5.292	37.17	2476-67-1	1.28	8.68	4.83	0.0066	0.032	0.012	
	13.40	5.427	24.58	2476-68-1		7.93					
	16.25	5.546	15.99	2476-68-2		7.97	4.73	0.0142	0.0288	0.0081	
	18.50	5.640	29.19	2476-70-1	1.29	8.75	4.71	0.0078	0.034	0.016	
	19.50	5.682	18.41	2476-70-3		7.6	4.95	0.0028	0.016	0.0057	
	20.45	5.721	34.70	2476-71-1		7.91	4.86	0.0027	0.015	0.0061	0.257
	21.45	5.763	20.37	2476-71-2	1.26	7.51	4.95	0.016	0.038	0.041	
	22.45	5.804	21.11	2476-71-3		7.83	5.08	0.007	0.025	0.014	
	23.45	5.846	32.48	2476-71-4	1.26	8.93	4.97	0.0041	0.019	0.0082	0.141
4-25-89	0.41	5.886	20.00	2476-72-1		7.92	4.97	0.0035	0.02	0.0074	
	3.10	5.998	22.81	2476-72-2	1.31	7.52	5.06	0.014	0.042	0.029	
	5.55	6.100	24.60	2476-73-1	1.29	8.37	4.94	0.0056	0.032	0.0099	
	8 1 2	6.207	19.40	2476-73-2		8.01	4.86	0.0035	0.018	0.007	
	8.43	6.220	20.00	2476-74-1		8.12	4.94	0.0043	0.024	0.0076	
	9.16	6.251	13.05	2476-74-2		8.18	4.95	0.0026	0.014	0.004	

TABLE A.2. Results from Analyses of Al Metal Samples

Date	Time	Event	Sample ID	Sample Weight	Cu	Fe	Ni
3–17–89	15.00	add metal		4701.00			
3–19–89	6.25	sample taken	2476–14–2	0.70	0.033	0.12	0.0047
	10.40	sample taken	2476–17–2	0.90	0.029	0.1	0.004
3–20–89	3.22	sample taken	2476–24–2	5.68	0.03	0.16	0.0088
	14.45	sample taken	2476–27–2	10.78	0.03	0.18	0.011
	23.05	sample taken	2476–31–2	1.80	0.04	0.19	0.026
	23.28	sample taken	2476–31–3	10.46	0.04	0.18	0.03
3–21–89	2.55	sample taken	2476–32–3	6.03	0.06	0.25	0.06
	6.07	sample taken	2476–34–1	2.85	0.09	0.38	0.11
	9.34	sample taken	2476–36–1	3.00	0.11	0.36	0.15
	15.16	sample taken	2476–38–2	3.74	0.16	0.48	0.24
	20.00	sample taken	2476–40–2	8.77	0.15	0.46	0.23
	22.50	sample taken	2476–43–2	10.06	0.19	0.52	0.28
3–22–89	2.59	sample taken	2476–45–1	2.27	0.27	0.69	0.49
	6.41	sample taken	2476–46–1	5.68	0.32	0.81	0.55
	9.20	sample taken	2476–47–1	4.42	0.41	0.99	0.69
	15.55	sample taken	2476–50–1	3.46	0.44	1.11	0.77
	19.47	sample taken	2476–52–2	5.35	0.51	1.26	0.86
3–23–89	4.37	sample taken	2476–56–1	2.00	0.62	1.5	1.04
	14.50	sample taken	2476–61–2	3.13	0.85	1.95	1.38
	19.20	sample taken	2476–62–2	4.45	0.86	1.86	1.31
3–24–89	0.20	sample taken	2476–64–2	2.50	0.97	2.105	1.505
	7.42	sample taken	2476–66–2	2.50	1.08	2.35	1.7
	12.20	sample taken	2476–67–2	5.43	1.12	2.48	1.76
	16.25	sample taken	2476–68–3	6.51	1.07	2.42	1.73
	18.50	sample taken	2476–70–2	4.67	1.15	2.53	1.82
3–25–89	6.03	sample taken	2476–73–2	3.00	1.6	3.28	2.53
	8.20	sample taken	2476–73–3	3.43	1.56	3.57	2.93
	10.00	sample taken	2476–74–3	3.00	1.4	3.43	2.33

4701.00	Initial Charge
6485	Bulk Recovery
126.60	Sample Amount Removed

DISTRIBUTION

No. of
Copies

OFFSITE

M. J. McMonigle
U.S. Department of Energy
Office of Industrial Programs
Forrestal Building
Washington, DC 20585

P. H. Salmon-Cox
U.S. Department of Energy
Office of Industrial Programs
Forrestal Building
Washington, DC 20585

12 DOE Office of Scientific and Technical Information

C. Anderson
Columbia Aluminum Co.
85 John Day Dam Road
Goldendale, WA 98620

J. V. Anderson
WCVE3
EG&G Idaho, Inc.
Idaho Falls, ID 83415

D. Auburg
Bonneville Power Administration
P.O. Box 3621, PDX 97208
Portland, OR 97208

F. W. Baker
Ceramics Division
Alcoa Laboratories
Alcoa Center, PA 15069

M. Baltzell
Eastalco Aluminum Company
Alumax, Inc.
5601 Manor Woods
Frederick, MD 21701

No. of
Copies

J. A. Barclay
U.S. Bureau of Mines
2401 "E" Street N.W.
Washington, DC 20241

H. Robert Baumgartner
Ceramics Division
Alcoa Laboratories
Alcoa Center, PA 15069

T. R. Beck
Electrochemical Technology Corp.
1601 Dexter Avenue
Seattle, WA 98109

S. Berwagan
Bonneville Power Administration
P.O. Box 3621 K
Portland, OR 97208

T. M. Besmann
Metals and Ceramics Division
Oak Ridge National Laboratory
P.O. Box X, Bldg. 4515
Oak Ridge, TN 37831-6063

K. A. Blakely
President
Advanced Refractory Technologies, Inc.
699 Hertel Ave.
Buffalo, NY 14207

M. H. Blenk
Du Pont
P.O. Box 787
Niagara Falls, NY 14302

No. of
Copies

L. G. Boxall
Martin Marietta Laboratories
1450 South Rolling
Baltimore, MD 21227

J. Bracher
Kaiser Aluminum and Chemical
Corp.
825 N.E. Multnomah St.,
Suite 960
Portland, OR 97232-2150

R. Brandt
Department of Materials Science
and Engineering
University of Washington FB-10
Seattle, WA 98195

J. J. Brown, Jr.
Materials Engineering
Virginia Polytechnic Institute
Blacksburg, VA 24061

A. Budner
Bonneville Power Administration
P.O. Box 3621--EPA
Portland, OR 97208

A. J. Caputo
Metals and Ceramics Division
Oak Ridge National Laboratory
P.O. Box X
Oak Ridge, TN 37831-6063

N. Clark
Bonneville Power Administration-
Industrial Conservation
P.O. Box 3621
Portland, OR 97208

A. Cooke
Martin Marietta Laboratories
1450 South Rolling
Baltimore, MD 21227

No. of
Copies

J. A. Coppola
Standard Oil Engineered
Materials Company
P.O. Box 156
Niagara Falls, NY 14302

D. D. Cudaback
Director
Washington State Dept of Trade
and Economic Development
312 First Avenue North
Seattle, WA 98109

R. Curtis
Materials Development
Corporation
81 Hicks Avenue
Medford, MA 02155

J. V. Day
Kaiser Aluminum and Chemical
Corp
E2111 Hawthorne Road
Mead, WA 99021

R. Dethlefsen
Maxwell Laboratories
8888 Balboa Ave
San Diego, CA 92123

D. H. DeYoung
Alcoa Technical Center
Alcoa Center, PA 15069

S. Diamond
Battelle Columbus Laboratories
505 King Avenue
Columbus, OH 43201-2693

C. W. Doerr
The Stackpole Corporation
Cermag Division
201 Stackpole Street
St. Marys, PA 15847

No. of
Copies

T. Dwonch
Snake River District
BPA
101 W. Poplar
Walla Walla, WA 99362

G. L. Eitel
Stone & Webster Engineering
Corp.
Greenwood Plaza Box 5406
Denver, CO 80217

R. Engdahl
Deposits and Composites, Inc.
318 Victory Drive
Herndon, VA 22070

J. F. Elliott
MIT
Room 4-138
77 Massachusetts Avenue
Cambridge, MA 02139

B. G. Epstein
A. D. Little, Inc.
955 Lenfant Plaza SW 4200
Washington, DC 20024-2119

J. W. Evans
University of California
Dept of Matl. Sci. and Mineral
Eng.
Berkeley, CA 94720

R. A. Fenimore
ICI Advanced Materials
Rollins Building, Eighth Floor
Wilmington, DE 19897

D. A. Figgins
ARCO Petroleum Products Co.
P.O. Box 61004
Anaheim, CA 92803-6104

No. of
Copies

P. Foster
Alcoa Laboratories
P.O. Box 772
New Kinsington, PA 15068

J. Gee
Great Lakes Research Corp
P.O. Box 1031
Elizabethton, TN 37643

T. Gilligan
Eltech Systems Corp.
625 East Street
Fairport Harbor, OH 44077

W. M. Goldberger
Superior Graphite Co.
120 S. Riverside Plaza
Chicago, IL 60606

J. Goodwell
Center for Metals Production
Mellon Institute
4400 Fifth Avenue
Pittsburgh, PA 15213

J.A.S. Green
Martin Marietta Laboratories
1450 South Rolling
Baltimore, MD 21227

C. Griffin
Ceramatec Inc.
2425 S. 900 West
Salt Lake City, UT 84119

L. [illegible] Grindstaff
Great Lakes Research Corp.
P.O. Box 1031
Elizabethon, TN 37643

J. Haggerty
MIT
Building 12, Room 009
77 Massachusetts Avenue
Cambridge, MA 02139

No. of
Copies

I. L. Harry
Electric Power Research
Institute
P.O. Box 10412
Palo Alto, CA 94303

W. E. Haupin
2820 7th Street Road
Lower Burrell, PA 15068

R. Hill
Union Carbide Corp.
P.O. Box 94637
Cleveland, OH 44101

H. F. Hillegass
Alcoa Wenatchee Works
P.O. Box 221
Wenatchee, WA 98807

D. G. Howitt
College of Engineering
University of California, Davis
Davis, CA 95616

F. R. Huettig
Advanced Magnetics, Inc.
45 Corey Lane
Mendham, NJ 07945

G. R. Hyde
U.S. Bureau of Mines
2401 "E" Street N.W.
Washington, DC 20241

S. C. Jacobs
Primary Processing
Aluminum Company of America
Alcoa Technical Center
Alcoa Center, PA 15069

S. H. Jan
Tennessee Valley Authority
R&D MR3A
1101 Market Street
Chattanooga, TN 37402-2801

No. of
Copies

N. Jarrett
149 Jefferson Avenue
New Kinsington, PA 15068

J. Johnson
Intalco Aluminum Company
P.O. Box 937
Ferndale, WA 98248

M. H. Johnson
Alcoa Wenatchee Works
P.O. Box 221
Wenatchee, WA 98801

L. Joo
Great Lakes Research Corp
P.O. Box 1031
Elizabethon, TN 37643

M. Karmous
Oregon State Department of
Energy
625 Marion Street, N.E.
Salem, OR 97310

R. Keller
RD 3 Roundtop Road
Export, PA 15632

K. Krupinski
Mail Stop 57
U.S. Steel Technical Center
1 Technical Center Drive
Monroeville, PA 15146

G. Y. Lai
Cabot Corporation
P.O. Box 9013
Kokomo, IN 46902-9013

R. A. Landy
Director of Research
North American Refractories Co.
3127 Research Dr.
State College, PA 16801

No. of
Copies

J. E. Lane
Ceramic Research and
Development Center
Westinghouse Electric
Corporation
1310 Beulah Road
Pittsburgh, PA 15235

Sai-Kwing Lau
Standard Oil Engineered
Materials Company
Niagara Falls R&D Center
P.O. Box 832
Niagara Falls, NY 14302

J. J. Leddy
Dow Chemical U.S.A.
1776 Building
Midland, MI 48640

W. W. Liang
Gas Research Institute
8600 West Bryne Mawr Avenue
Chicago, IL 60631

W. H. Link
Columbia Aluminum Corp.
85 John Day Dam Road
Goldendale, WA 98620

Steve Loftness
Washington State Energy Office
400 E. Union
Olympia, WA 98504

W. Long
Building B815
Dow Chemical
Freeport, Texas 77541

A. G. Longmuir
Kaiser Aluminum and Chemical
Corp.
P.O. Box 877
Pleasonton, CA 94566

No. of
Copies

R. A. Lowden
Metals and Ceramics Division
Oak Ridge National Laboratory
P.O. Box X, Bldg, 4515
Oak Ridge, TN 37831-6063

W. N. Maclay
Koppers Company, Inc.
440 College Park Drive
Monroeville, PA 15146

J. C. McCloskey
Ten Mile River Associates
296 Mt. Hope Street
North Attleboro, MA 02760

S. C. Manaktala
Manager of Technology
Reduction Division
Kaiser Aluminum and Chemical
Corp
300 Lakeside Drive
Oakland, CA 94643

V. H. Markant
Du Pont
P.O. Box 787
Niagara Falls, NY 14302

C. J. McMinn
Extractive Metallurgical
Department
Reynolds Metals Company
P.O. Box 1200
Sheffield, AL 35660

C. H. McMurtry
Standard Oil Engineered
Materials Company
Niagara Falls R&D Center
P.O. Box 832
Niagara Falls, NY 14302

M. A. Mitnick
Avco Specialty Materials
Subsidiary of Textron Inc.
2 Industrial Avenue
Lowell, MA 01851

No. of
Copies

H. Mortensen
R. Palika
Cercom, Inc.
P.O. Box 70
Vista, CA 92083

A. Moussa
A. D. Little, Inc.
20 Acorn Park
Cambridge, MA 02140

B. C. Mutsuddy
Battelle Columbus Division
505 King Avenue
Columbus, OH 43201-2693

P. Ness
Senior Project Manager
Washington State Dept of Trade and Economic Development
312 First Avenue North
Seattle, WA 98109

A. N. Patel
Battelle Columbus Laboratories
505 King Avenue
Columbus, OH 43201-2693

J. R. Payne
Kaiser Aluminum and Chemical Corp.
P.O. Box 877
Pleasanton, CA 94566

T. Payne
Columbia Falls Aluminum Co.
Columbia Falls, MT

W. Pebley
Oregon Freeze Dry Corp.
525 25th Avenue SW
P.O. Box 1048
Albany, OR 97321

No. of
Copies

K. Peterson
Columbia Aluminum Corp.
85 John Day Dam Road
Goldendale, WA 98620

R. D. Peterson
Reynolds Metals Company
P.O. Box 1200
Sheffield, AL 35660

T. R. Pritchett
Kaiser Aluminum and Chemical Corp.
P.O. Box 877

W. W. Pritsky
Aluminum Association
900 19th St. N.W.
Washington, DC 20006

S. P. Ray
Alcoa Technical Center
Alcoa Center, PA 15069

J. F. Rhodes
Advanced Composite Materials Corp.
1525 S. Buncomb Rd.
Greer, SC 29651

N. E. Richards
Reduction Laboratory
Reynolds Aluminum Corporation
P.O. Box 1200
Sheffield, AL 35660

J. J. Ritter
Ceramics Division
National Bureau of Standards
Gaithersburg, MD 20899

R. C. Rohwedder
3028 Ohio Street
Longview, WA

No. of
Copies

J. Rosling
Myers Metals and Minerals
459 Colman Building
Seattle, WA 98104

D. R. Sadoway
MIT
Room 8-109
77 Massachusetts Avenue
Cambridge, MA 02139

W. Scott
Department of Materials Science
& Engineering
Wilcox Hall FB-10
University of Washington
Seattle, WA 98195

D. R. Secrist
Great Lakes Research Corp.
P.O. Box 1031
Elizabethon, TN 37643

A. B. Shah
Noranda Aluminum, Inc.
P.O. Box 70
New Madras, MO 63869

N. Shelton
Intalco
1300 S. W. 5th, Suite 3508
Portland, OR 97201

F. W. Spillers
Dow Chemical U.S.A.
B-1210 Building
Freeport, TX 77541

R. M. Spriggs
Office of the Director
Center for Advanced
Ceramic Technology
Alfred University
Alfred, NY 14802

No. of
Copies

D. V. Stewart
Reynolds Metals Co.
P.O. Box 1200
Sheffield, AL 35660

D. Strahan
Reynolds Metals Company
P.O. Box 27003
Richmond, VA 23261

A. T. Tabereaux
Reynolds Metals Company
P.O. Box 1200
Sheffield, AL 35660

G. P. Tarcy
Aluminum Company of America
Alcoa Technical Center
Alcoa Center, PA 15069

P. Thaure
Primary Planning and Production
Alumax
400 S. El Camino Rd.
San Mateo, CA 94402

W. H. Thielbahr
Conservative Technology
Division
DOE-Idaho Operations Office
785 DOE Place
Idaho Falls, ID 83402

S. Thomson
General Manager
Klickitat PUD
1313 S. Columbus
Goldendale, WA 98620

R. Unger
Merner Research
P.O. Box 248
Ridgewood, NJ 07451

No. of
Copies

A. Vinnard
Bonneville Power Administration
(KWI)
P.O. Box 3621
Portland, OR 97208

T. Von Muller-KWI
Bonneville Power Administration
P.O. Box 3621
Portland, OR 97208

D. H. Weinblatt
AIMCOR
One Parkway North
Deerfield, IL 60015

J. D. Weyand
EG&G Idaho, Inc.
Idaho Falls, ID 83415

B. Wilcox
Northwest Aluminum Co.
3313 W. Second St.
The Dalles, OR 97058

C. B. Wilson
Dow Chemical U.S. A.
Texas Operations
B-101 Building
Freeport, TX 77541

J. C. Withers
Keramont Research Corporation
4233 S. Fremont Avenue
Tucson, AZ 85714

W. A. Zdaniewski
Engelhard Corporation
Menlo Park, CN 28
Edison, NJ 08818

FOREIGN

D. Brodie
Comalco Ltd.
55 Collins St.
Melbourne, AUSTRALIA

No. of
Copies

H. Connor
Group Licensing Controller
Johnson Matthey, plc
New Garden House
78 Hatton Garden
London EC1N 8JP ENGLAND

L. Dion
Alcan International Limited
C.P. 6090
Montreal, Quebec
CANADA, H3C 3H2

T. Kjar
Comalco Ltd.
55 Collins St.
Melbourne, AUSTRALIA

E. W. Dewing
Alcan International
P.O. Box 8400
Kingston, Ontario
CANADA K7L 4Z4

D. N. MacMillan
Alcan International
C.P. 1250
Jonquieve, Quebec
CANADA G7S 4K8

J. H. Reimers
Jan H. Reimers and Associates
Inc.
221 Lakeshore Road East
Oakville, Ontario
CANADA, L6J 1H7

A. Oye
Institute of Inorganic Chemistry
Norwegian Institute of Technology
University of Trondheim
N-7034 Trondheim-NTH, NORWAY

No. of
Copies

J. Thonstad
Laboratories of Industrial
Electrochemistry
Norwegian Institute of
Technology
University of Trondheim
N-7034 Trondheim-NTH, NORWAY

K. O. Vee
ASV Ardal Verk
N-5875 Ardalstargen, NORWAY

ONSITE

DOE Richland Operations Office

R. B. Goranson A5-90

No. of
Copies

25 Pacific Northwest Laboratory

M. Clement K1-17
N. C. Davis P8-35
D. K. Hilliard K2-12
G. L. McVay K2-45
N. L. Moore K6-54
L. G. Morgan (10) K2-35
C. H. Schilling K2-44
D. M. Strachan K2-44
R. E. Westerman P8-37
C. F. Windisch P8-37
Publishing Coordination
Technical Report Files (5)